Supporting Information

Indolylbenzothiadiazoles as highly tunable fluorophores for imaging lipid droplet accumulation in astrocytes and glioblastoma cells

Kilian Colas,[1] Karl O. Holmberg,[2] Linus Chiang,[3] Susanne Doloczki,[1] Fredrik J. Swartling[2] and Christine Dyrager[1,*]

[1]Department of Chemistry - BMC, Uppsala University, SE-751 23 Uppsala, Sweden
[2]Department of Immunology, Genetics and Pathology, Science for Life Laboratory, Uppsala University, SE-751 85, Uppsala, Sweden
[3]Department of Chemistry, University of the Fraser Valley, BC V2S 7M8 Abbotsford, Canada

Contents

General Information

Materials. All reagents and solvents were purchased from Sigma-Aldrich or Fluorochem and used without further purification. All solvents used for synthesis were obtained from VWR Chemicals and used without further purification. For photophysical characterization, DMSO and chloroform of spectroscopic grade were purchased from VWR Chemicals; THF and toluene from VWR Chemicals were distilled before use. For reactions performed at room temperature: 18 °C ≤ r.t. ≤ 23 °C.

Chromatography. Thin-layer chromatography (TLC) was carried out using aluminum plates coated with silica gel ($60F_{254}$, Merck) and visualized through exposure to UV light (λ = 254 nm and 365 nm). Flash silica gel column chromatography was performed using silica gel (particle size 40–63 μm, VWR Chemicals).

Characterization. NMR spectra for the characterization of compounds were recorded at 298 K on a Varian Unity instrument 400 MHz (^{1}H) and at 101 MHZ (^{13}C) and 377 MHZ (^{19}F). Chemical shifts (δ) are reported in ppm using the residual solvent peak in $CDCl_3$ (δ_H = 7.26 and δ_C = 77.2 ppm) or DMSO (δ_H = 2.50 and δ_C = 39.5 ppm) as internal reference;[1] in the case of ^{19}F spectra chemical shifts were calibrated to an external standard at 0.00 ppm ($CFCl_3$). Coupling constants (J) are given in Hz and the apparent resonance multiplicity is reported as s (singlet), d (doublet), t (triplet), q (quartet), p (pentet), h (hexet), hept (heptet), or m (multiplet). High-resolution mass spectrometry (HRMS) data was determined at Imperial College London, Molecular Characterization Facility, Department of Chemistry, London, UK. UV/Vis absorption spectra were acquired on a UV-1650PC Shimadzu instrument at room temperature using quartz cuvettes (10 mm). Absorption maxima (λ_{max}) are reported in nm with the molar extinction coefficient (ε) in M^{-1} cm^{-1} with a margin of error of 0 to 6 %. For each compound three data points with known different concentrations were acquired and the measured absorbances (≤1) were plotted against the concentrations. The molar extinction coefficient was then determined according to the Beer-Lambert law as the slope of the linear fit. Fluorescence measurements were carried out using a Spex Fluorolog 1680 0.22m Double Spectrometer instrument. Fluorescence quantum yields (Φ_F) were determined relative to fluorescein in 20 mM aq. NaOH (Φ_F = 0.93)[2] or quinine sulfate in 0.1 M aq. H_2SO_4 (Φ_F = 0.55).[3] Three fluorescence spectra were recorded per compound per solvent, and the area under the curved were plotted against the absorbances at the excitation wavelength. The quantum yields were then calculated from the slope of the linear fit *via* the comparative method, with a margin of error of 0 to 10%. Refractive indices of solvents were adjusted for quantum yield calculations based on the excitation wavelength used.[4–6] The excitation wavelength (360 or 430 nm) and concentrations for the quantum yield measurements were selected so that the absorbance was below 0.1 to prevent self-absorption effects. Obtained raw data was processed using OriginPro 8 software. Emission spectra illustrated herein were normalized to the peak maximum of interest and smoothed using an FFT filter function with 5 point window.

Cell Cultures

SK-MEL-28 (ATCC® HTB-27™), U1242MG (kind gift from Professor Bengt Westermark) and Normal Human Astrocytes (NHA) (3H Biomedical, Cat#SC1800) were grown in DMEM, high glucose, GlutaMAX™ (Thermo Fisher Scientific, Cat#61965026) supplemented with 10% heat inactivated Fetal Bovine Serum (Thermo Fisher Scientific, Cat#10270106) and Penicilin-Streptomycin (Sigma-Aldrich, Cat#P0781) using 100 mm TC treated dishes (VWR, Cat#734-0006) and a humidified incubator at 37°C with 5% CO_2. Cells were passaged using Trypsin – EDTA Solution (Sigma-Aldrich, Cat#T3924) after washing with Dulbecco's Phosphate-Buffered Saline (DPBS) (Thermo Fisher Scientific, Cat#14190094).

Cell Viability Assay

Cells were counted using a Countess II Automated Cell Counter (ThermoFisher Scientific, Cat#AMQAX1000) and seeded in 96 well plates, 10 000 live cells/well, the day before treatment. Compounds were diluted in Dimethyl Sulfoxide (DMSO) (Sigma-Aldrich, Cat#317275) as 2 mM stock solutions. Cells were incubated with compounds for 24 hours at a final concentration of 10μM (for a final DMSO concentration of *ca.* 0.15%) with DMSO treated cells as control. Cell viability was analyzed after 2.5 hours incubation with Resazurin Reagent (1:10) (Sigma-Aldrich, Cat#R7017) using a Synergy™ HTX Multi-Mode Reader (BioTek), fluorescence was detected by excitation at 530 nm and emission at 590 nm. Experiments were run in triplicates and repeated twice.

Cell Staining (Fluorescent staining)

Cells were counted (as mentioned above) and seeded in chamber slides (Sarstedt, Cat#94.6140.802) the day before treatment at following densities; SK-MEL-28 and U1242MG; 80 000 live cells/well, NHA; 65 000 live cells/well. Cells were incubated with compounds at a final concentration of 10μM for 24 hours with DMSO treated cells as control, fixated using a 4% Buffered Formaldehyde Solution (Histolab Cat#02176) for 15 minutes at room temperature, followed by incubation with DAPI (1:1000) (Sigma-Aldrich, Cat#D9564) diluted in Tris-Buffered Saline (VWR, Cat# 97062-370) with 1% TWEEN® 20 (Sigma-Aldrich, Cat#P1379) (TBST) for 15 minutes at room temperature. Cells not stained with DAPI were incubated with TBST alone. Slides were then washed in TBST and mounted using Fluoromount (Sigma-Aldrich, Cat#F4680). Stainings were performed twice for each compound to ensure reproducibility, photos were taken using a Leica DMi8 microscope. Different filters (channels) were used for visualizing the fluorescence; Blue channel (ex 325-375nm, em 435-485 nm), green channel (ex 460-500 nm, em 512-542 nm), yellow channel (ex 532-558 nm, em 570-640 nm) and red channel (ex 590-650nm, em 662-738nm).

Colocalization experiments with compound **11** in melanoma cells were performed using Anti-ADFP antibody [EPR3713] from Abcam (ab108323). Anti-rabbit IgG Fab2 Alexa FluorR 647 from Cell Signaling (Cat#4414S) was used as secondary antibody. A stock solution of the compound in DMSO was prepared at 2.5 mM concentration. Live cells were incubated with compounds at a final concentration of 10 μM for 24 hours (*i.e.*, 0.4 vol% DMSO). The cells were washed using PBS, followed by fixation using a 4% Buffered Formaldehyde Solution (Histolab Cat#02176) for 15 minutes at room temperature. Subsequently, cells were permeabilized with 0.2% Triton X/ PBS for 5 min at 4 °C, washed with PBS (×2), and blocked with 0.5% BSA/ PBS for 30 min at room temperature. The cells were then incubated with the primary antibody diluted in 0.5% BSA/ PBS (200 μL; 1:1000) for 2 h at room temperature, washed with PBS (3 × 5 min), followed by incubation with secondary antibody (1:1000) together with DAPI (1:1000) diluted in 0.5% BSA/ PBS (200 μL) for 1 h at room temperature, washing

with PBS (3 × 5 min) and mounting using Fluoromount (Sigma-Aldrich, Cat#F4680). Images were taken on a Zeiss LSM700 confocal microscope and processed using ImageJ.

BBB scores calculation

The BBB scores were calculated by uploading the chemical structures of the compounds into the online platform CBLigand developed by Xie *et. al*. (https://www.cbligand.org/BBB/) as part of the AlzPlatform system.[7] The presented scores were obtained using the default parameters: support vector machine (SVM) algorithm and Molecular ACCess System (MACCS) fingerprints. The results were cross-checked with all other available combinations of parameters, confirming the BBB+ character of all compounds in this study.

I – Synthetic procedures

General procedure A for the Suzuki coupling reactions

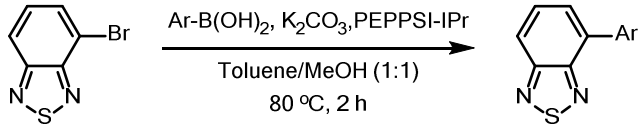

The procedure was adapted from reported literature as follows:[8] to a solution of 4-Bromo-2,1,3-benzothiadiazole (100 mg, 0.47 mmol, 1.0 equiv.) and K_2CO_3 (190 mg, 1.38 mmol, 3.2 equiv.) in toluene/methanol (1:1, 14 mL), the relevant arylboronic acid or boronate ester (0.94 mmol, 2.0 equiv.) and PEPPSI-IPr (6.3 mg, 2 mol%) were added. The reaction mixture was stirred at 80 °C for 2 h, then allowed to cool down to r.t.. The reaction mixture was diluted with water (50 mL) and extracted with EtOAc (3 × 30 mL). The combined organic layers were washed with brine (2 × 30 mL), dried over Na_2SO_4 and concentrated *in vacuo*. The crude product was purified by column chromatography.

General procedure B for the Boc-deprotection of *N*-Boc-indole-BTD derivatives

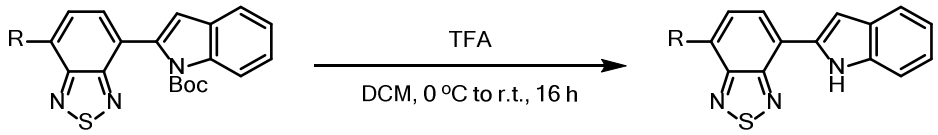

To a solution of the relevant BTD-indole derivative (1.38 mmol) in CH_2Cl_2 (20 mL) stirred at 0 °C, trifluoroacetic acid (TFA) (4 mL, 50 mmol) was added. The resulting solution was allowed to reach r.t. and was stirred overnight (*ca*. 16 h). The reaction was quenched with sat. aq. $NaHCO_3$ (100 mL) and extracted with CH_2Cl_2 (2 × 30 mL). The combined organic layers were washed with brine (2 × 50 mL), dried over Na_2SO_4 and concentrated *in vacuo*. The resulting crude products dried under high vacuum for 16 h and were deemed of sufficient purity (as judged by NMR) to be used without further purification.

General procedure C for the *N*-functionalization of *N*-H-indole-BTD derivatives

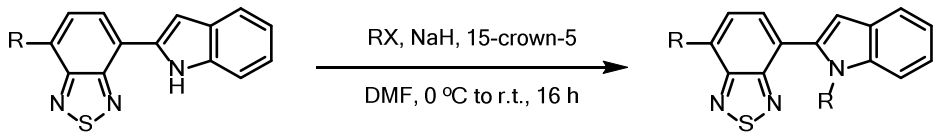

To a solution of the relevant BTD-indole derivative (0.1 mmol) in DMF (2 mL) stirred at 0 °C, NaH (5 mg, 0.12 mmol, 1.2 equiv.) was added. The resulting deep, bright purple solution was allowed to reach r.t. and stirred for 30 min, then 15-crown-5 (22 mg, 0.1 mmol, 1.0 equiv) and the relevant electrophile (1.5 mmol, 1.5 equiv.) were added. The resulting solution was stirred overnight at r.t. – 65 °C, as indicated. The reaction was quenched with water (10 mL) and extracted with EtOAc (3 × 10 mL). The combined organic layers were washed with brine (3 × 50 mL), dried over Na_2SO_4 and concentrated *in vacuo*. The crude product was purified by column chromatography.

4-(1*H*-indol-2-yl)benzo[c][1,2,5]thiadiazole (1).

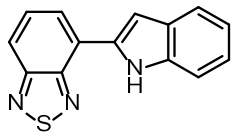

1

The compound was synthesized from **5** (481 mg, 1.38 mmol), following the general procedure B (described above) , yielding **1** as a brown solid (345 mg, 99 %) whose characterization data was in accordance with reported literature.[9] The purity (as judged by NMR) was deemed sufficient and the compound was used without further purification. ^{1}H NMR (400 MHz, $CDCl_3$) δ = 10.83 (br s, 1H), 8.10 – 8.03 (m, 1H), 7.92 – 7.88 (m, 1H), 7.72 – 7.61 (m, 2H), 7.55 – 7.50 (m, 1H), 7.29 – 7.23 (m, 1H), 7.22 – 7.13 (m, 2H); ^{13}C NMR (101 MHz, $CDCl_3$) δ =155.6, 151.9, 137.1, 134.6, 129.9, 128.2, 124.6, 124.5, 123.0, 120.9, 120.3, 119.7, 111.5, 100.9.

4-(1-methyl-1*H*-indol-2-yl)benzo[c][1,2,5]thiadiazole (2).

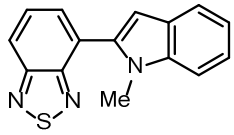

2

The compound was synthesized according to the general procedure A (described above) using *N*-methyl-indole-2-boronic acid pinacol ester (237 mg, 0.92 mmol, 2.0 equiv.). The crude mixture was recrystallized from hexane to provide **2** as a fluorescent orange solid (103 mg, 84 %). ^{1}H NMR (400 MHz, $CDCl_3$) δ = 8.12 – 8.06 (m, 1H), 7.77 – 7.73 (m, 1H), 7.72 – 7.68 (m, 2H), 7.48 – 7.45 (m, 1H), 7.38 – 7.33 (m, 1H), 7.25 – 7.20 (m, 1H), 6.90 (s, 1H), 3.74 (s, 3H); ^{13}C NMR (101 MHz, $CDCl_3$) δ = 155.2, 153.9, 138.8, 136.9, 130.1, 129.4, 128.0, 126.4, 122.4, 121.4, 121.0, 120.0, 109.8, 104.6, 31.9**;** HR-MS: (ESI-TOF) calcd for $[C_{15}H_{11}N_3S + H]^+$ 266.0752; found 266.0749.

4-(1-isopropyl-1*H*-indol-2-yl)benzo[c][1,2,5]thiadiazole (3).

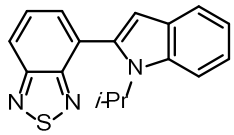

3

The compound was synthesized from **1** (25 mg, 0.1 mmol), according to the general procedure C (described above), using isopropyl bromide (31 mg, 0.12 mmol, 1.2 equiv.) at 65 °C. The crude mixture was recrystallized from hexane to provide **3** as a dark orange solid (5 mg, 18 %). ^{1}H NMR (400 MHz, $CDCl_3$) δ = 8.08 (dd, *J* = 8.6, 1.3 Hz, 1H), 7.71 – 7.63 (m, 4H), 7.26 – 7.21 (m, 1H), 7.16 – 7.11 (m, 1H), 6.66 (s, 1H), 4.39 (hept, *J* = 7.0 Hz, 1H), 1.62 (d, *J* = 7.0 Hz, 6H); ^{13}C NMR (101 MHz, $CDCl_3$) δ = 155.0, 154.4, 136.4, 135.8, 130.5, 129.3, 129.1, 127.3, 121.6, 121.5, 121.3, 119.5, 112.5, 104.2, 49.1, 21.4; HR-MS: (ESI-TOF) calcd for $[C_{17}H_{15}N_3S + H]^+$ 294.1059; found 294.1063.

1-(2-(benzo[c][1,2,5]thiadiazol-4-yl)-1*H*-indol-1-yl)ethan-1-one (4).

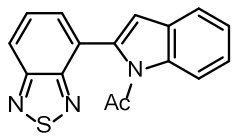

4

The compound was synthesized from **1** (25 mg, 0.1 mmol), following the general procedure C (described above), using acetyl chloride (12 mg, 0.15 mmol, 1.5 equiv.) at r.t.. The crude mixture was purified by column chromatography (pentane/ CH_2Cl_2 1:4, R_f =0.17) to provide **4** as a yellow solid (21 mg, 72 %).[1]H NMR (400 MHz, $CDCl_3$) δ= 8.27 (d, *J* = 8.5 Hz, 1H), 8.07 (dd, *J* = 8.5, 1.4 Hz, 1H), 7.76 – 7.67 (m, 2H), 7.63 (d, *J* = 7.8 Hz, 1H), 7.45 – 7.38 (m, 1H), 7.35 – 7.29 (m, 1H), 6.88 (d, *J* = 0.8 Hz, 1H), 2.17 (s, 3H); ^{13}C NMR (101 MHz, $CDCl_3$) δ = 170.6, 154.9, 153.6, 137.5, 135.4, 129.5, 129.0, 128.3, 127.9, 125.5, 123.5, 121.8, 121.0, 115.5, 113.4, 26.6; HR-MS: (ESI-TOF) calcd for $[C_{16}H_{11}N_3OS + H]^+$ 294.0696; found 294.0694.

***N*-Boc-2-(benzo[c][1,2,5]thiadiazol-4-yl)-indole (5).**

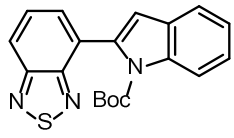

5

The compound was synthesized according to the general procedure B (described above) using *N*-Boc-indole-2-boronic acid (240 mg, 0.92 mmol, 2.0 equiv.). Purification by column chromatography (hexane/CH_2Cl_2 1:1, R_f = 0.23) gave **5** as a fluorescent yellow solid (147 mg, 91 %) whose characterization data was in accordance with reported literature.[9] ^{1}H NMR (400 MHz, $CDCl_3$) δ= 8.31 (d, *J* = 8.4 Hz, 1H), 8.06 – 7.99 (m, 1H),7.69 – 7.65 (m, 2H), 7.64 – 7.60 (m, 1H), 7.43 – 7.36 (m, 1H), 7.32 – 7.26 (m, 1H), 6.78 (s, 1H), 1.08 (s, 9H); ^{13}C NMR (101 MHz, $CDCl_3$) δ= 154.8, 154.2, 149.9, 137.6, 135.8, 129.5, 129.0, 128.9, 127.5, 124.9, 123.0, 121.1, 120.8, 115.5, 111.3, 83.0, 27.4.

(2-(benzo[c][1,2,5]thiadiazol-4-yl)-1*H*-indol-1-yl)(phenyl)methanone (6).

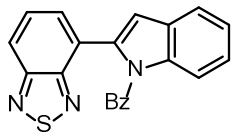

6

The compound was synthesized from **1** (25 mg, 0.1 mmol), following the general procedure C (described above), using benzoyl chloride (21 mg, 0.15 mmol, 1.5 equiv.) at r.t.. The crude mixture was purified by column chromatography (Toluene/EtOAc/CH_2Cl_2 15:1:1, R_f = 0.53) to provide **6** as a sticky yellow solid (29 mg, 83 %). **^{1}H** NMR (400 MHz, $CDCl_3$) δ= 7.79 (d, *J* = 8.8 Hz, 1H), 7.71 – 7.64 (m, 3H), 7.55 – 7.48 (m, 3H), 7.32 – 7.26 (m, 3H), 7.14 – 7.08 (m, 2H), 7.01 (s, 1H); ^{13}C NMR (101 MHz, $CDCl_3$) δ= 169.9, 154.6, 152.8, 138.3, 136.7, 134.8, 132.4, 129.5, 129.2, 129.0, 128.2, 127.7, 127.2, 124.9, 123.2, 121.0, 121.0, 114.5, 111.7. HR-MS: (ESI-TOF) calcd for $[C_{21}H_{13}N_3OS + H]^+$ 356.0858; found 356.0860.

4-(1-tosyl-1*H*-indol-2-yl)benzo[c][1,2,5]thiadiazole (7).

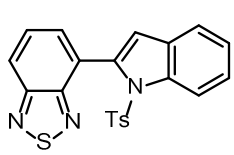

7

The compound was synthesized from **1** (25 mg, 0.1 mmol), following the general procedure C (described above), using tosyl chloride (29 mg, 0.15 mmol, 1.5 equiv.) at 120 °C. The crude mixture was purified by column chromatography (pentane/ CH_2Cl_2 1:4, R_f =0.27) to provide **7** as an orange solid (21 mg, 52 %). Note: the product was observed as a mixture of rotamers (major:minor = *ca.* 10:1) in the NMR spectra. ^{1}H NMR (400 MHz, $CDCl_3$) δ_{major} =8.29 (d, *J* = 8.4 Hz, 1H), 8.09 (d, *J* = 8.4 Hz, 1H), 7.78 -7.69 (m, 2H), 7.52 (d, *J* = 8.0 Hz, 1H), 7.42 – 7.36 (m, 1H), 7.32 – 7.26 (m, 1H), 7.26 – 7.23 (m, 2H), 6.99 – 6.95 (m, 2H), 6.92 (s, 1H), 2.26 (s, 3H); ^{13}C NMR (101 MHz, $CDCl_3$) δ_{major} = 154.7, 154.2, 144.7, 138.2, 136.5, 134.5, 131.1, 130.3, 129.2, 128.8, 126.7, 125.8, 125.3, 124.3, 122.0, 121.2, 116.4, 115.4, 21.5; HR-MS: (ESI-TOF) calcd for $[C_{21}H_{15}N_3O_2S_2 + H]^+$ 406.0678; found 406.0677.

(9*H*-fluoren-9-yl)methyl-2-(benzo[c][1,2,5]thiadiazol-4-yl)-1*H*-indole-1-carboxylate (8).

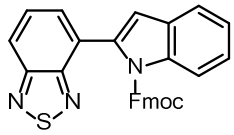

8

The compound was synthesized from **1** (25 mg, 0.1 mmol), following the general procedure C (described above), using Fmoc chloride (31 mg, 0.12 mmol, 1.2 equiv.) at r.t.. Purification by column chromatography (CH_2Cl_2, R_f = 0.55) gave **8** as a fluorescent yellow solid (12 mg, 26 %). ^{1}H NMR (400 MHz, $CDCl_3$) δ = 7.98 – 7.94 (m, 1H), 7,91 – 7.86 (m, 1H), 7.74 – 7.70 (m, 3H), 7.65 – 7.59 (m, 2H), 7.41 – 7.32 (m, 5 H), 7.30 – 7.26 (m, 2H), 7.25 – 7.22 (m, 1H), 6.85 (s, 1H), 4.43 (d, *J* = 6.3 Hz, 2H), 3.64 (t, *J* = 6.3 Hz, 1H); ^{13}C NMR (101 MHz, $CDCl_3$) δ = 154.7, 153.9, 151.5, 143.0, 141.2, 137.2, 135.9, 129.3, 129.1, 128.0, 127.9, 127.6, 127.2, 125.2, 124.7, 123.3, 121.5, 120.9, 120.0, 115.5, 112.3, 68.7, 46.4; HR-MS: (ESI-TOF) calcd for $[C_{29}H_{19}N_3O_2S + H]^+$ 474.1276; found 474.1281.

4-(7-(1*H*-indol-2-yl)benzo[c][1,2,5]thiadiazol-4-yl)-*N*,*N*-dimethylaniline (9).

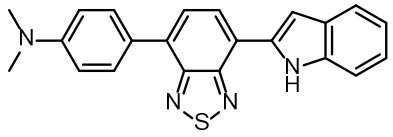

9

The compound was synthesized from **12** (135 mg, 0.29 mmol), following the general procedure B (described above), yielding **9** as a dark red solid (103 mg, 96 %). The purity (as judged by NMR) was deemed sufficient, and the compound was used without further purification. ^{1}H NMR (400 MHz, $CDCl_3$) δ = 10.92 (br s, 1H), 8.14 (d, *J* = 7.6 Hz, 1H), 7.94 (d, *J* = 8.5 Hz, 2H), 7.72 (d, *J* = 7.6 Hz, 1H), 7.69 (d, *J* = 8.1 Hz, 1H), 7.53 (d, *J* = 8.1 Hz, 1H), 7.26 – 7.21 (m, 1H), 7.19 (s, 1H),7.17 – 7.12 (m, 1H), 6.89 (d, *J* = 8.5 Hz, 2H), 3.06 (s, 6H); ^{13}C NMR (101 MHz, $CDCl_3$) δ = 154.2, 152.9, 150.6, 137.0, 135.2, 132.9, 130.0, 128.4, 126.4, 125.6, 124.9, 122.6, 121.7, 120.6, 120.2, 112.3, 111.4, 100.1, 40.4; HR-MS: (ESI-TOF) calcd for $[C_{22}H_{18}N_4S + H]^+$ 371.1325; found 371.1322.

***N*,*N*-dimethyl-4-(7-(1-methyl-1*H*-indol-2-yl)benzo[c][1,2,5]thiadiazol-4-yl)aniline (10).**

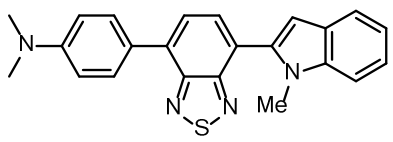

10

The compound was synthesized from **9** (37 mg, 0.1 mmol), following the general procedure C (described above), using methyl iodide (10 µL, 0.15 mmol, 1.5 equiv.) at r.t. for 1 h. The crude mixture was purified by column chromatography (CH_2Cl_2, R_f =0.56) to provide **10** as an orange solid (14 mg, 36 %). ^{1}H NMR (400 MHz, $CDCl_3$) δ = 7.99 – 7.94 (m, 2H), 7.76 – 7.71 (m, 2H), 7.70 (dd, *J* = 7.9, 1.0 Hz, 1H), 7.43 (dd, *J* = 8.3, 1.0 Hz, 1H), 7.33 – 7.26 (m, 1H), 7.20 – 7.14 (m, 1H), 6.93 – 6.88 (m, 2H), 6.85 (s, 1H), 3.75 (s, 3H), 3.07 (s, 6H); ^{13}C NMR (101 MHz, $CDCl_3$) δ = 155.7, 153.9, 150.7, 138.7, 137.5, 134.5, 130.8, 130.1, 128.0, 125.7, 124.9, 123.4, 122.1, 120.8, 119.9, 112.3, 109.7, 104.0, 40.4, 31.9; HR-MS: (ESI-TOF) calcd for $[C_{23}H_{20}N_4S + H]^+$ 385.1481; found 385.1469.

1-(2-(7-(4-(dimethylamino)phenyl)benzo[c][1,2,5]thiadiazol-4-yl)-1*H*-indol-1-yl)ethan-1-one (11).

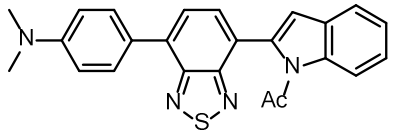

11

The compound was synthesized from **9** (37 mg, 0.1 mmol), following the general procedure C described above, using acetyl chloride (12 mg, 0.15 mmol, 1.5 equiv.) at r.t. for 2 h. The crude mixture was purified by column chromatography (Toluene/EtOAc/CH_2Cl_2 15:1:1, R_f = 0.38) to provide **11** as a yellow solid (37 mg, 90 %). ^{1}H NMR (400 MHz, $CDCl_3$) δ = 8.33 – 8.30 (m, 1H), 7.98 – 7.94 (m, 2H), 7.76 (dd, *J* = 12.2, 7.3 Hz, 2H), 7.64 – 7.61 (m, 1H), 7.43 – 7.38 (m, 1H), 7.33 – 7.28 (m, 1H), 6.92 – 9.86 (m, 3H), 3.07 (s, 6 H), 2.17 (s, 3H); ^{13}C NMR (101 MHz, $CDCl_3$) δ = 171.0, 154.4, 153.6, 150.8, 137.6, 135.9, 134.9, 130.1, 129.2, 129.1, 125.7, 125.3, 124.7, 124.6, 123.5, 120.8, 115.7, 113.0, 112.3, 40.4, 26.7; HR-MS: (ESI-TOF) calcd for $[C_{24}H_{20}N_4OS + H]^+$ 413.1431; found 413.1422.

***N*-Boc-2-(7-(4-(dimethylamino)phenyl)benzo[c][1,2,5]thiadiazol-4-yl)-indole (12).**

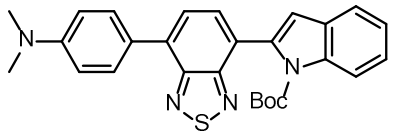

12

The compound was synthesized from **13** (100 mg, 0.30 mmol) following the general procedure A (described above) using *N*-Boc-indole-2-boronic acid (86 mg, 0.33 mmol, 1.1 equiv.). Purification by column chromatography (hexane/CH_2Cl_2 1:2, R_f = 0.60) gave **12** as a fluorescent yellow solid (140 mg, 99 %). ^{1}H NMR (400 MHz, $CDCl_3$) δ = 8.29 (d, *J* = 8.4 Hz, 1H), 7.95 (d, *J* = 8.8 Hz, 2H), 7.73 – 7.69 (m, 2H), 7.62 (d, *J* = 7.7 Hz, 1H), 7.40 – 7.36 (m, 1H), 7.31 – 7.26 (m, 1H), 6.91 (d, *J* = 8.8 Hz, 2H), 6.79 (s, 1H), 3.06 (s, 6H), 1.10 (s, 9H); ^{13}C NMR (101 MHz, $CDCl_3$) δ = 155.0, 153.6, 150.6, 150.0, 137.5, 136.3, 134.2, 130.1, 129.1, 128.2, 126.1, 125.8, 125.1, 124.7, 122.9, 120.7, 115.4, 112.3, 110.9, 83.0, 40.4, 27.5; HR-MS: (ESI-TOF) calcd for $[C_{27}H_{26}N_4O_2S + H]^+$ 471.1855; found 471.1845.

4-(7-bromobenzo[c][1,2,5]thiadiazol-4-yl)-*N*,*N*-dimethylaniline (13).

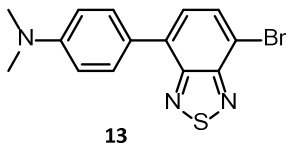

13

The compound was prepared as described in the literature using 4,7-dibromo-2,1,3-benzothiadiazole (201 mg, 0.68 mmol).[10] The crude mixture was purified by column chromatography (CH_2Cl_2, R_f =0.47) to provide **13** as an orange solid (147 mg, 65%) whose characterization data was in accordance with the reported literature.[10] ^{1}H NMR (400 MHz, $CDCl_3$) δ = 7.87 – 7.81 (m, 3H), 7.48 (d, *J* = 7.7 Hz, 1H), 6.85 (d, J = 8.9 Hz, 2H), 3.04 (s, 6H).

II – Absorption and Emission spectra

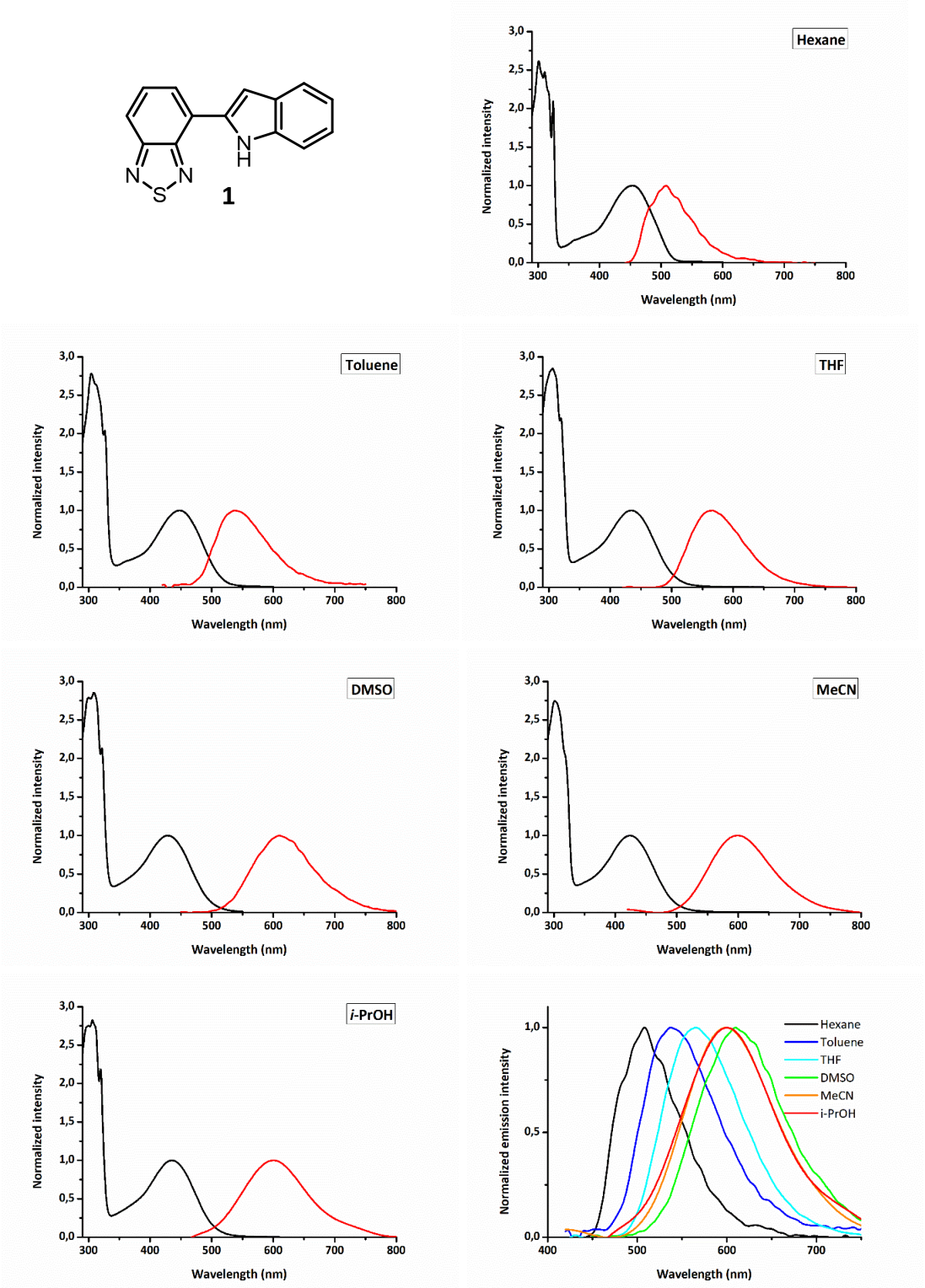

Figure S1: Normalized UV absorption (black) and emission (red) spectra of **1** in various solvents. The bottom right spectrum shows the combined emission spectra to visualize solvatochromism.

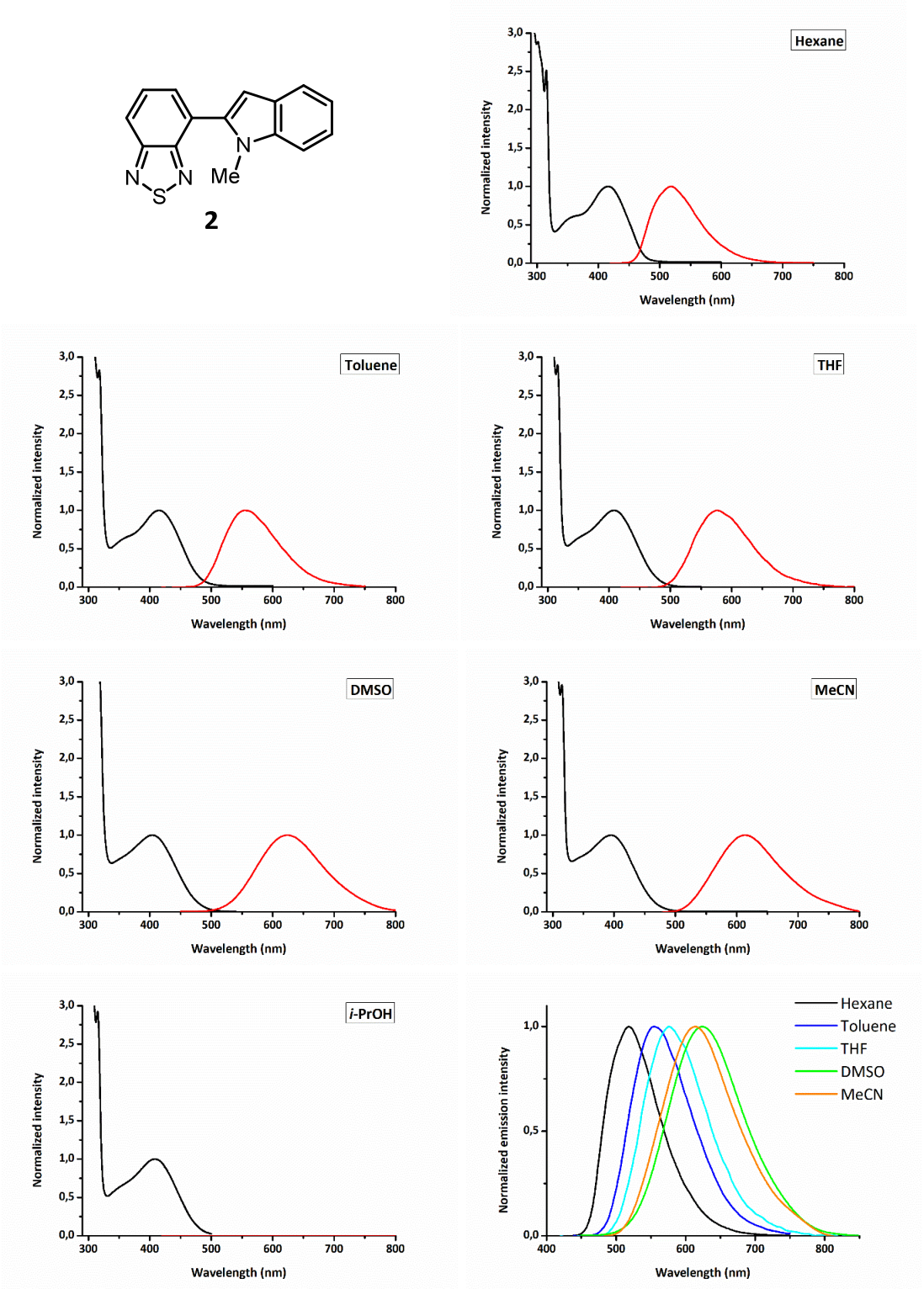

Figure S2: Normalized UV absorption (black) and emission (red) spectra of **2** in various solvents. No emission was observed in *i*-PrOH. The bottom right spectrum shows the combined emission spectra to visualize solvatochromism.

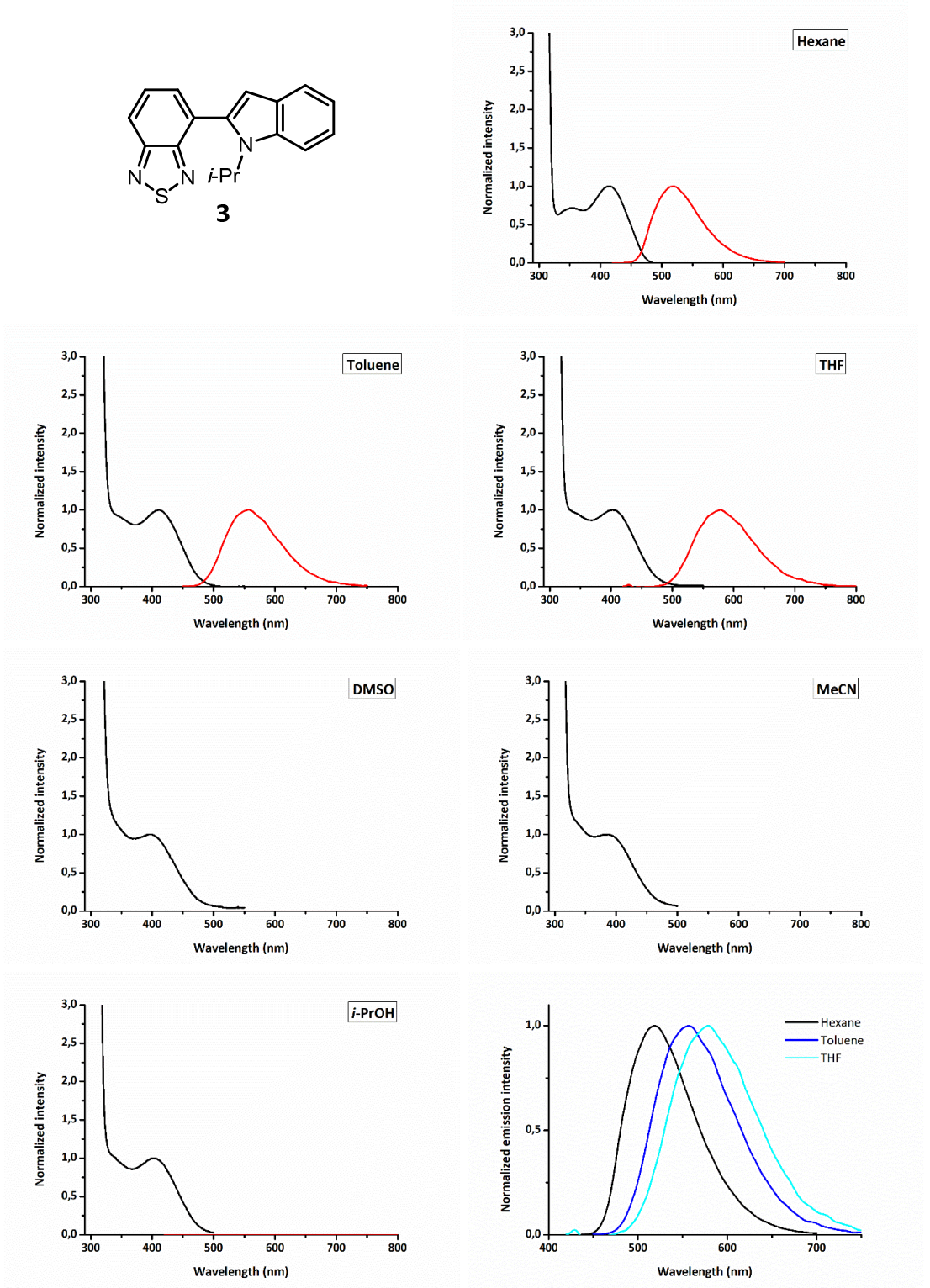

Figure S3: Normalized UV absorption (black) and emission (red) spectra of **3** in various solvents. No emission was observed in DMSO, MeCN or *i*-PrOH. The bottom right spectrum shows the combined emission spectra to visualize solvatochromism.

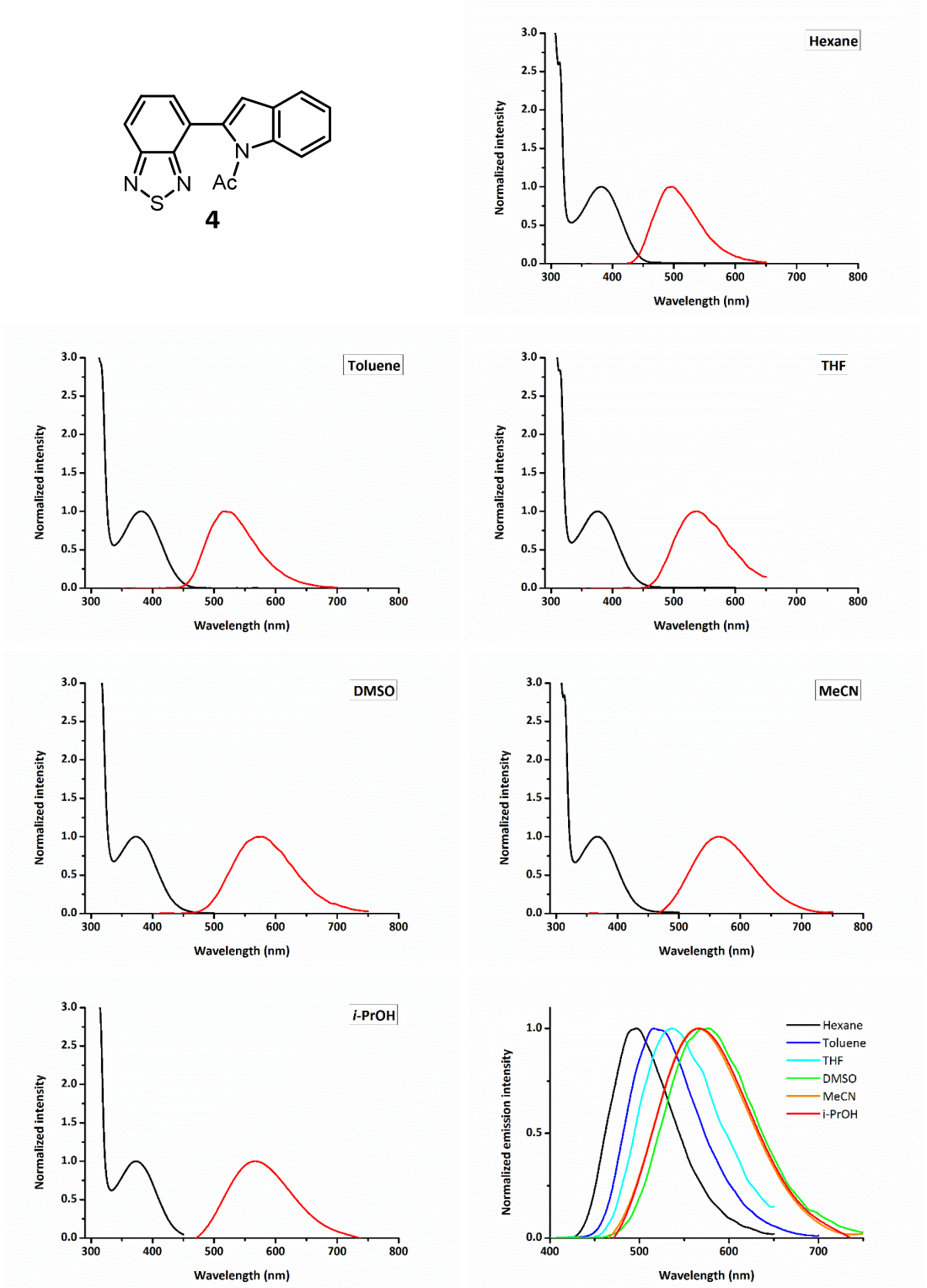

Figure S4: Normalized UV absorption (black) and emission (red) spectra of **4** in various solvents. The bottom right spectrum shows the combined emission spectra to visualize solvatochromism.

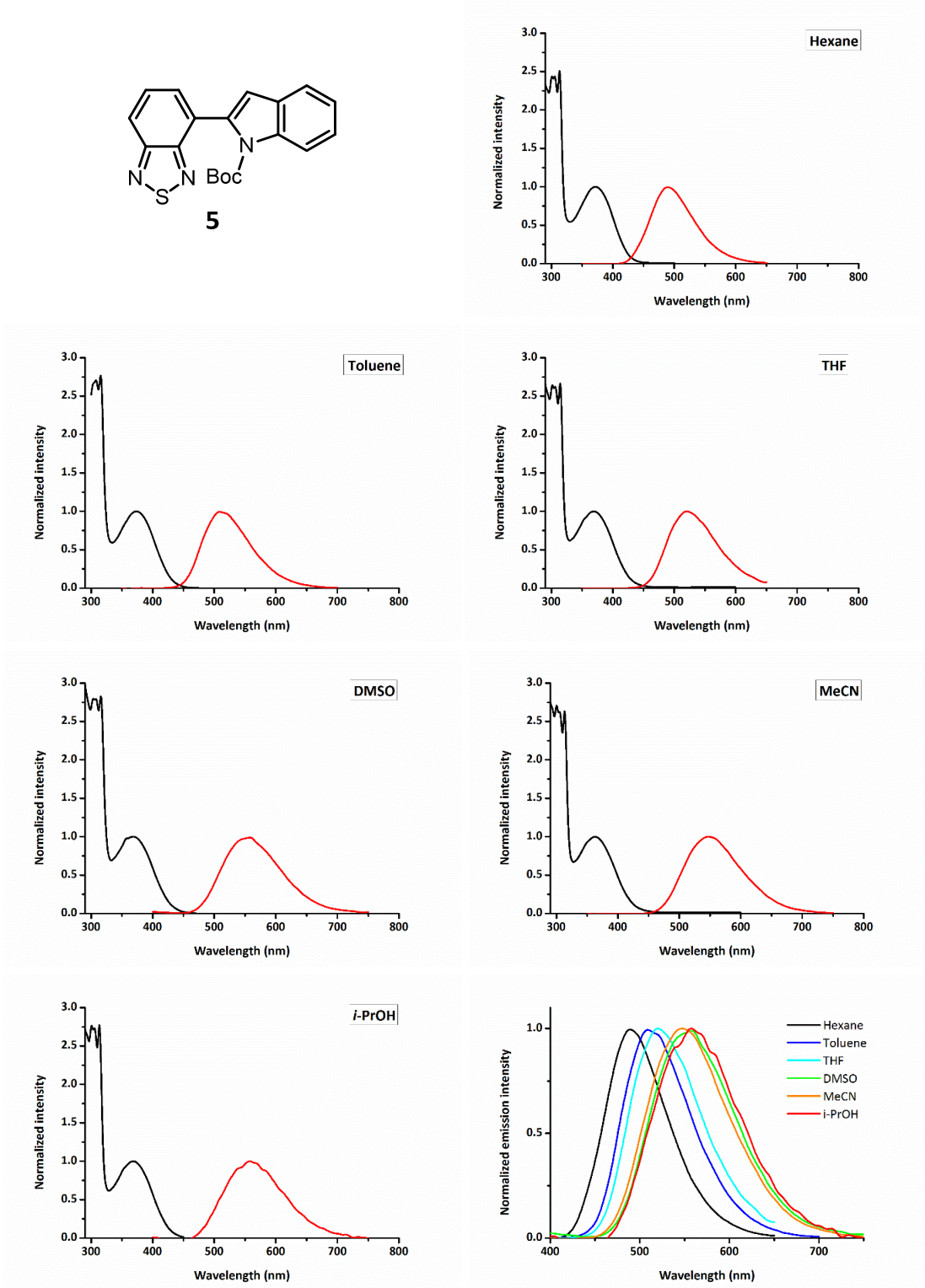

Figure S5: Normalized UV absorption (black) and emission (red) spectra of **5** in various solvents. The bottom right spectrum shows the combined emission spectra to visualize solvatochromism.

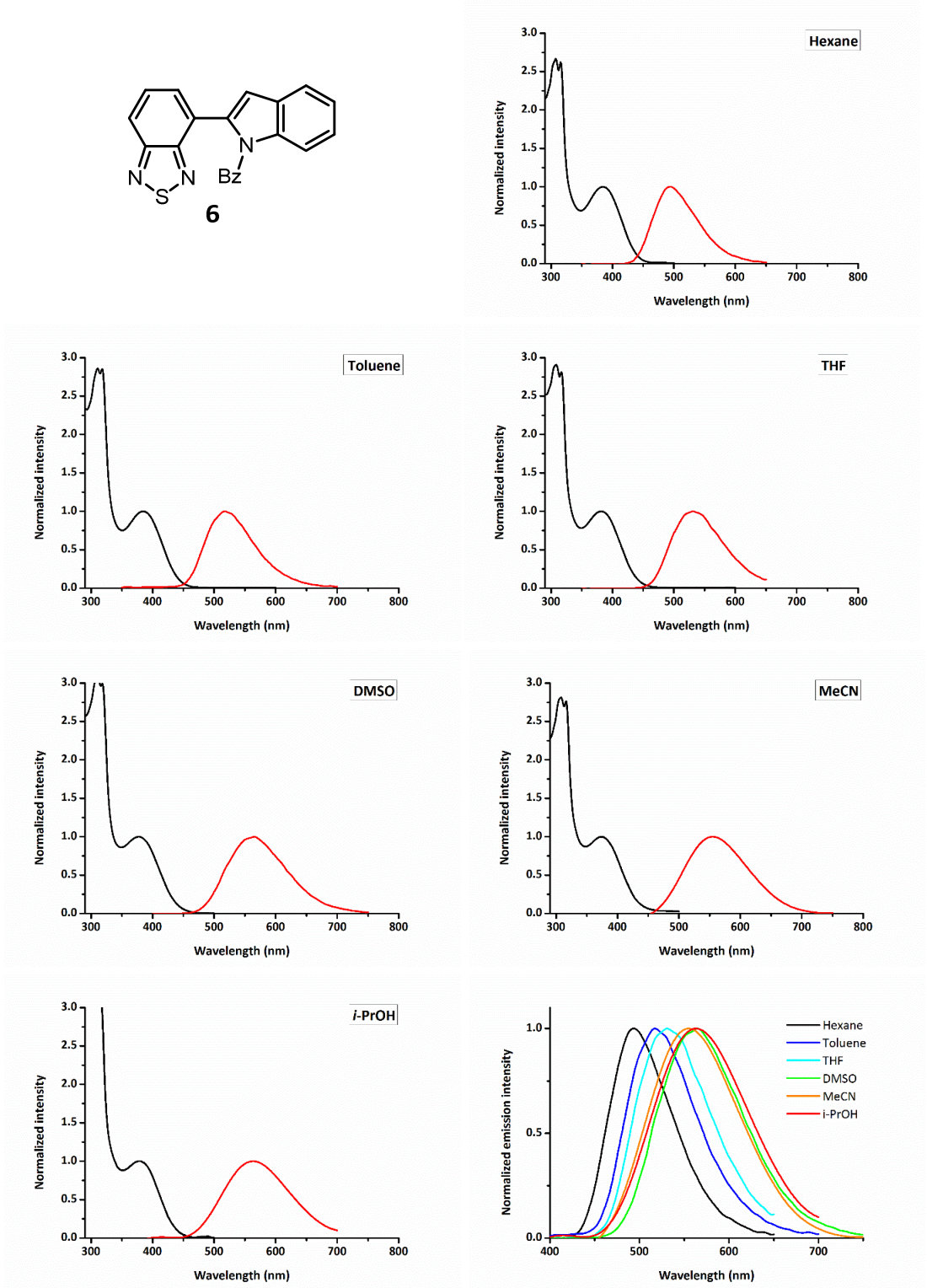

Figure S6: Normalized UV absorption (black) and emission (red) spectra of **6** in various solvents. The bottom right spectrum shows the combined emission spectra to visualize solvatochromism.

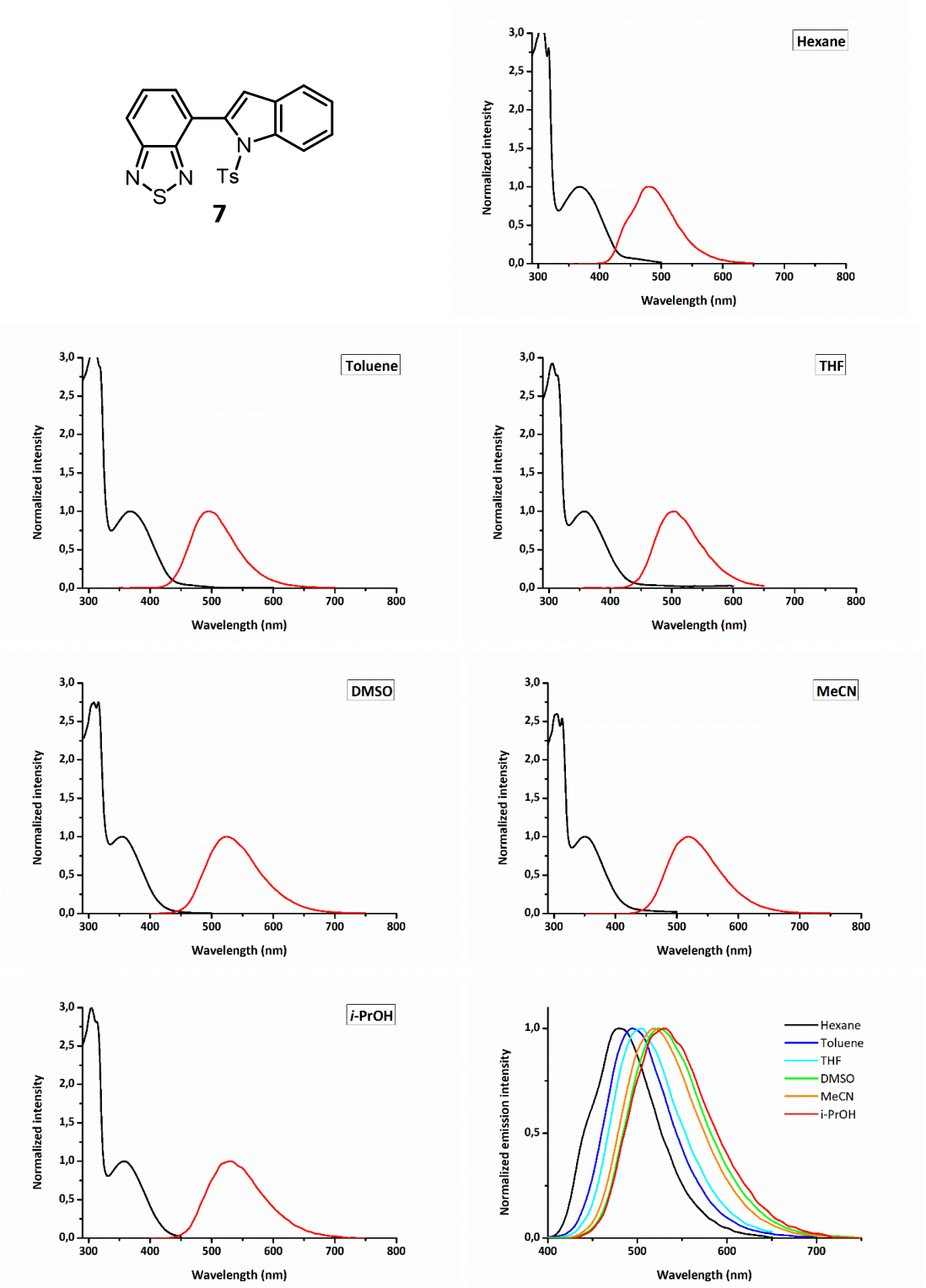

Figure S7: Normalized UV absorption (black) and emission (red) spectra of **7** in various solvents. The bottom right spectrum shows the combined emission spectra to visualize solvatochromism.

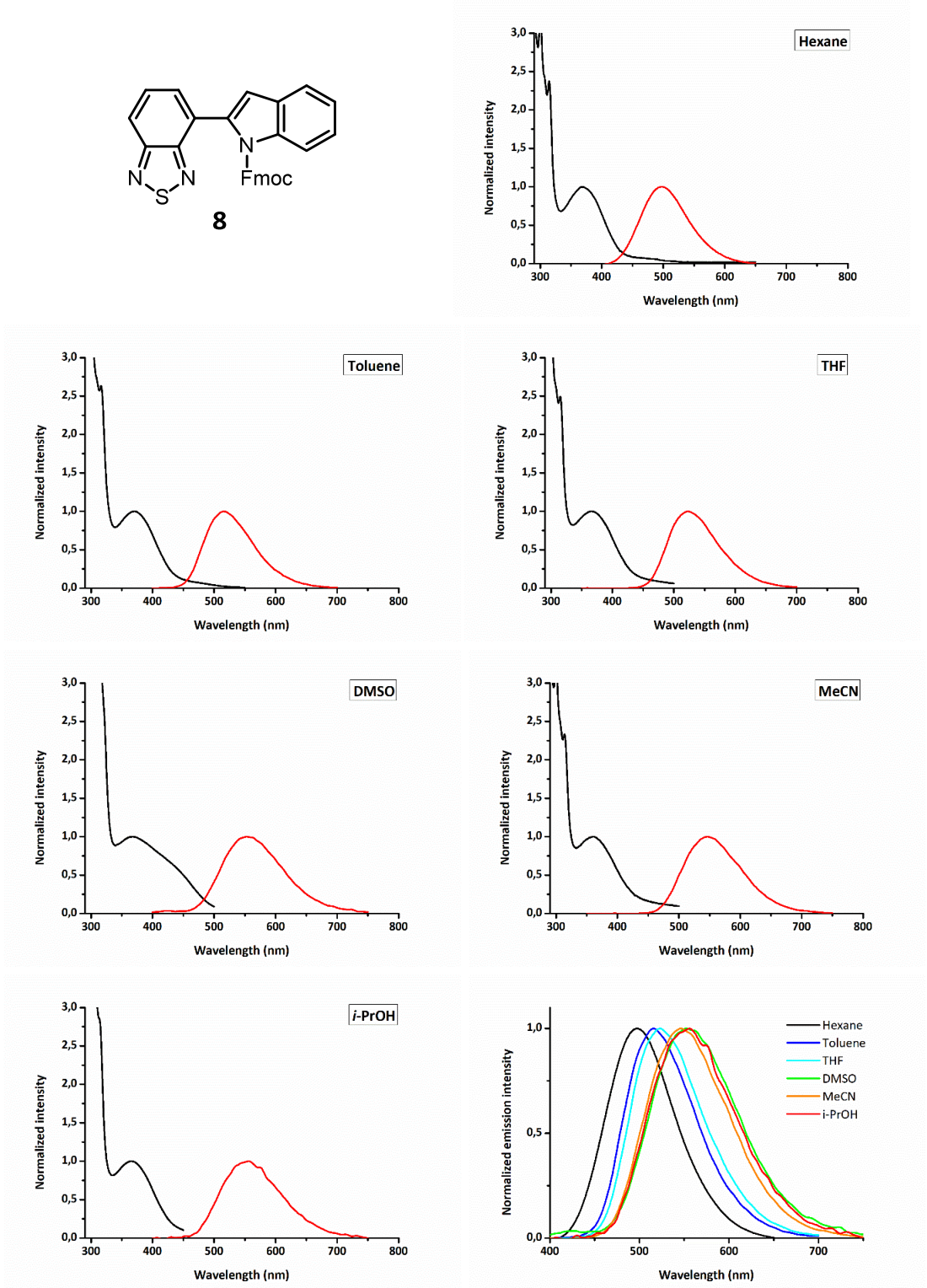

Figure S8: Normalized UV absorption (black) and emission (red) spectra of **8** in various solvents. The bottom right spectrum shows the combined emission spectra to visualize solvatochromism.

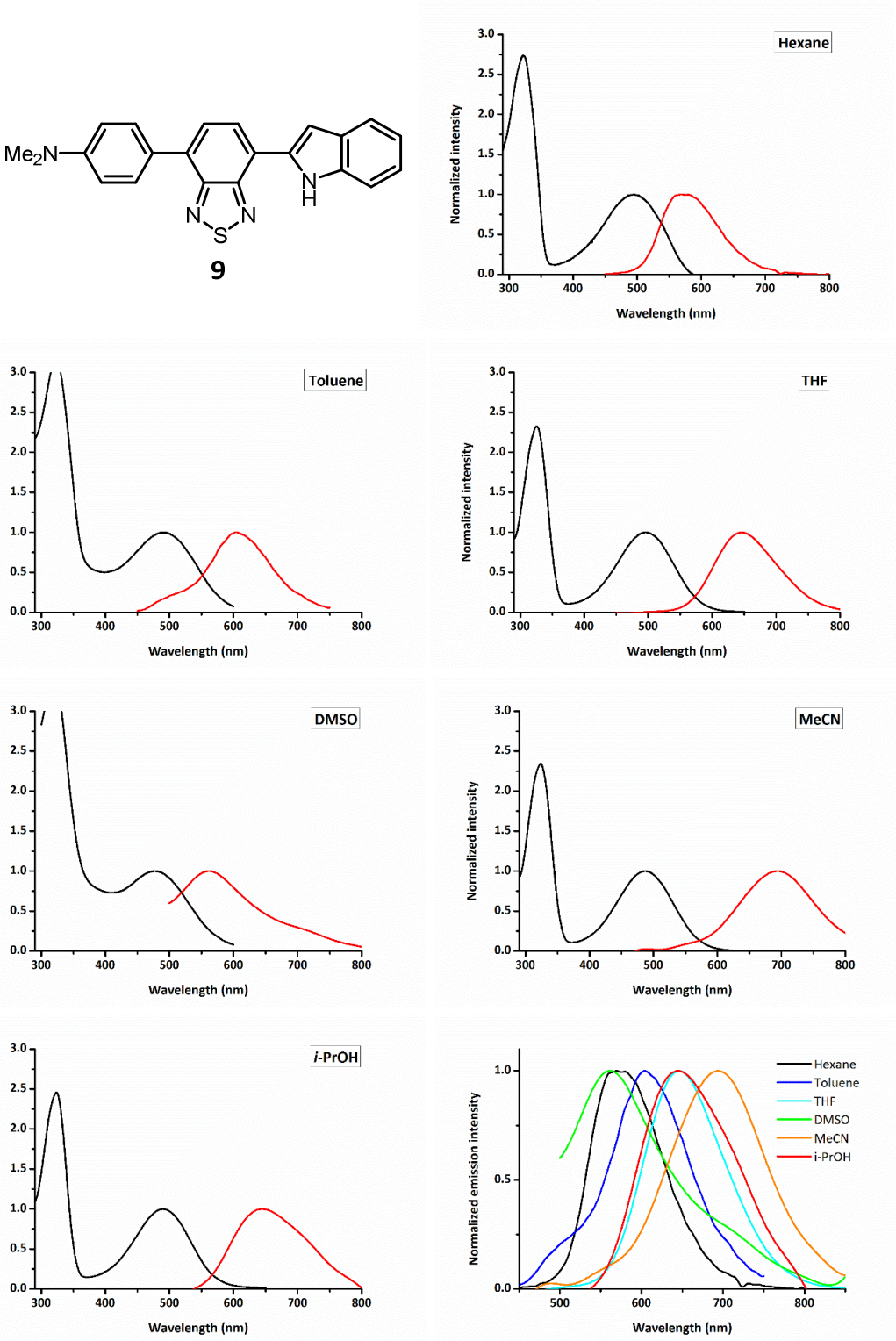

Figure S9: Normalized UV absorption (black) and emission (red) spectra of **9** in various solvents. The bottom right spectrum shows the combined emission spectra to visualize solvatochromism.

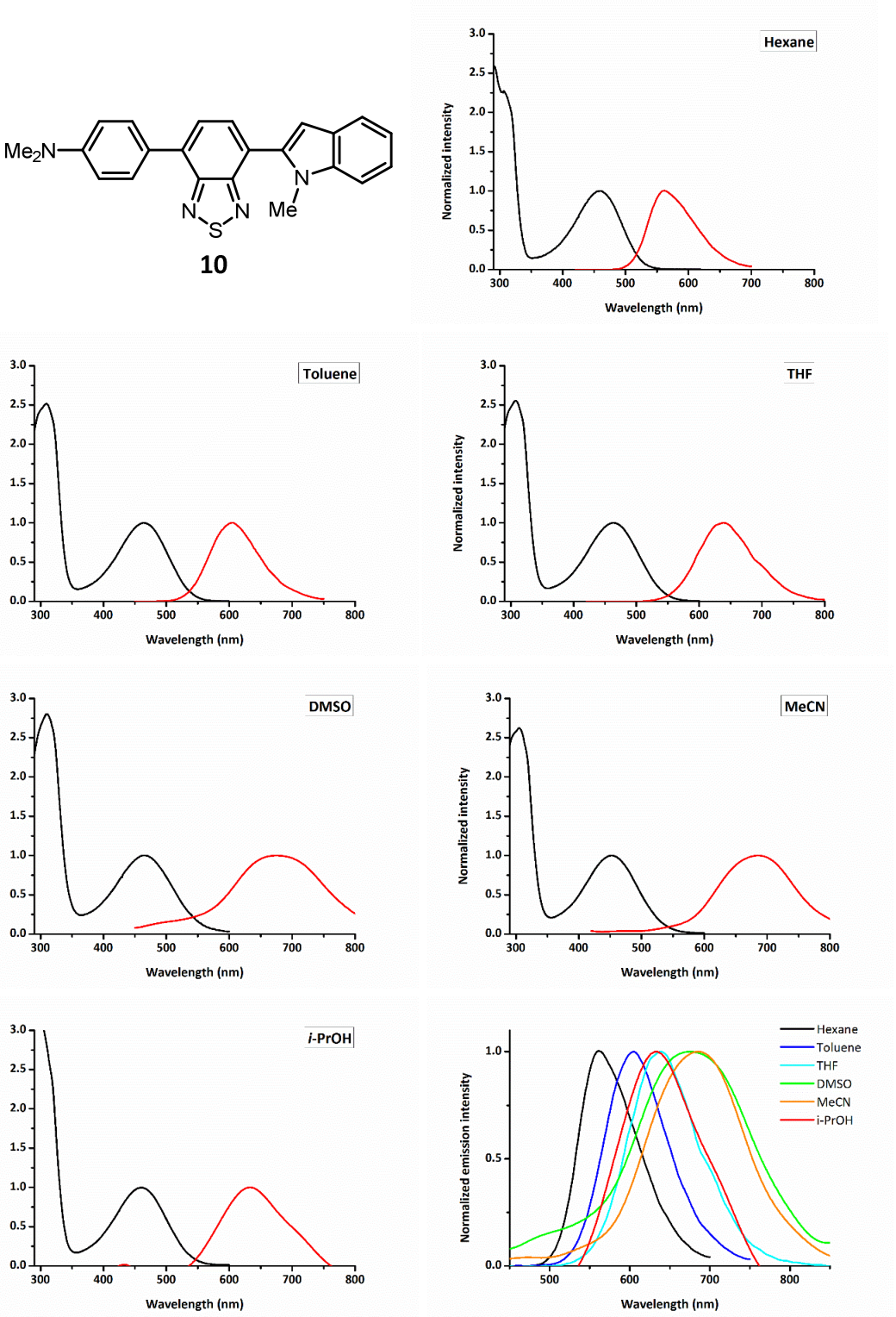

Figure S10: Normalized UV absorption (black) and emission (red) spectra of **10** in various solvents. The bottom right spectrum shows the combined emission spectra to visualize solvatochromism.

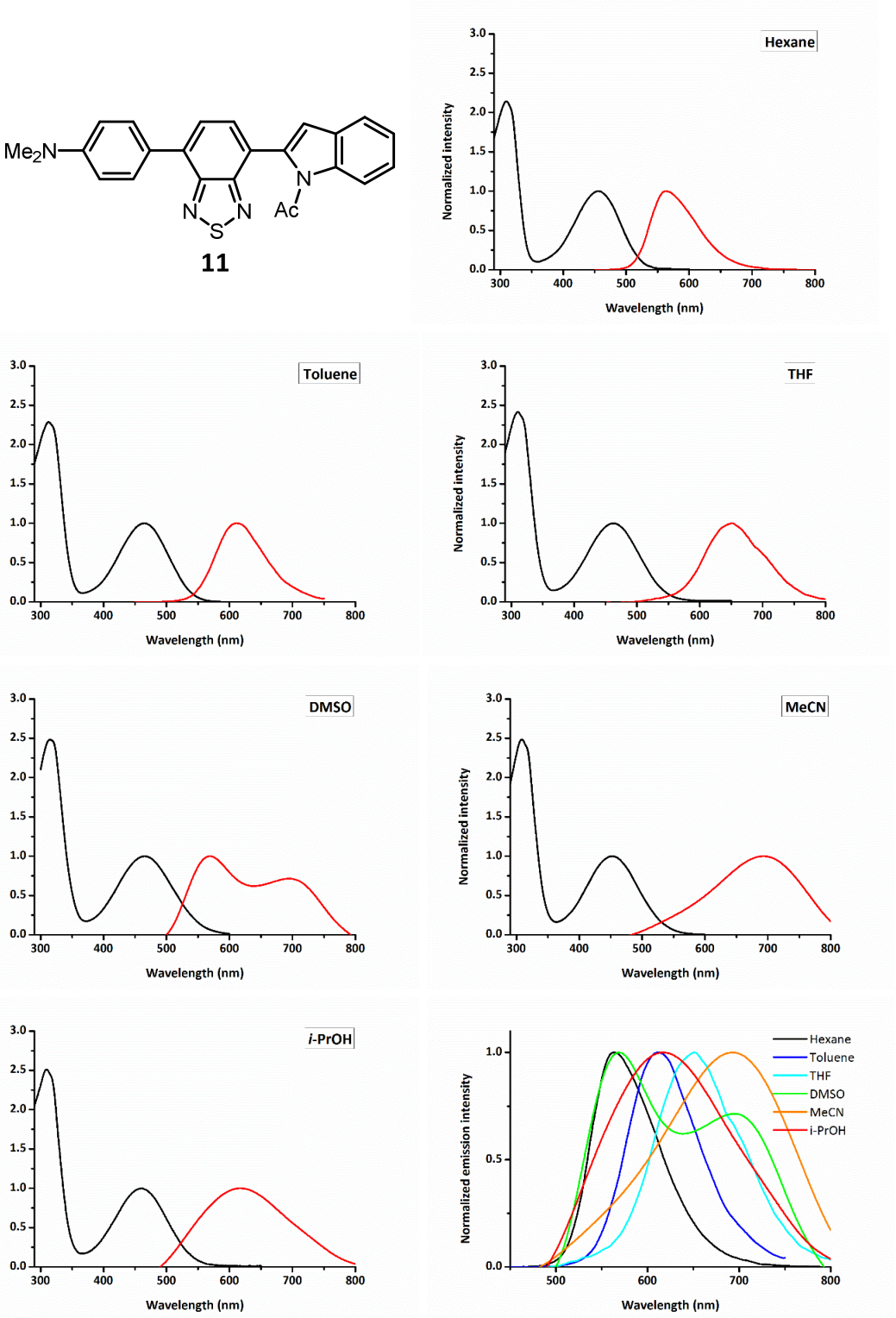

Figure S11: Normalized UV absorption (black) and emission (red) spectra of **11** in various solvents. The bottom right spectrum shows the combined emission spectra to visualize solvatochromism.

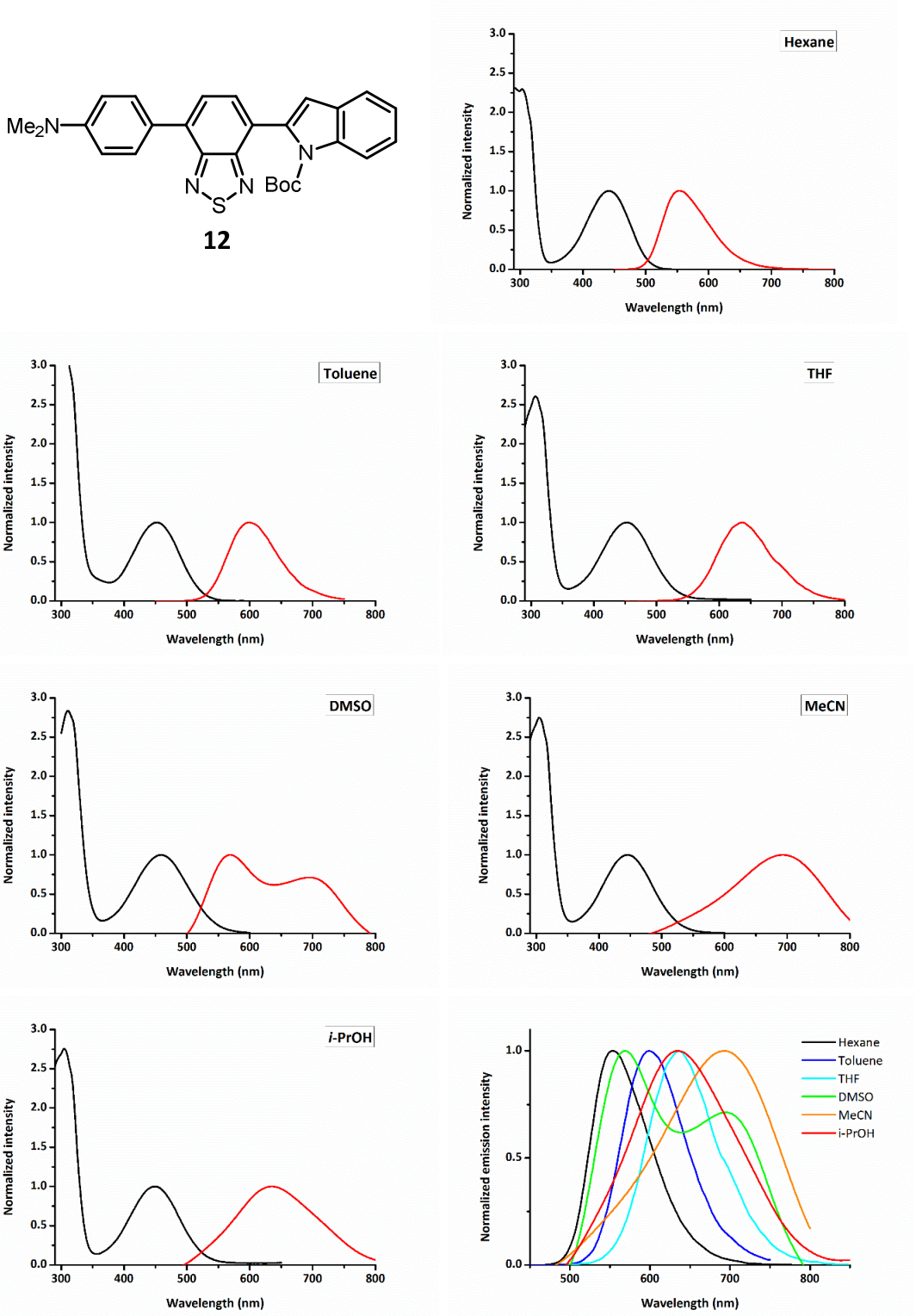

Figure S12: Normalized UV absorption (black) and emission (red) spectra of **12** in various solvents. The bottom right spectrum shows the combined emission spectra to visualize solvatochromism.

III – Lippert-Mataga plots

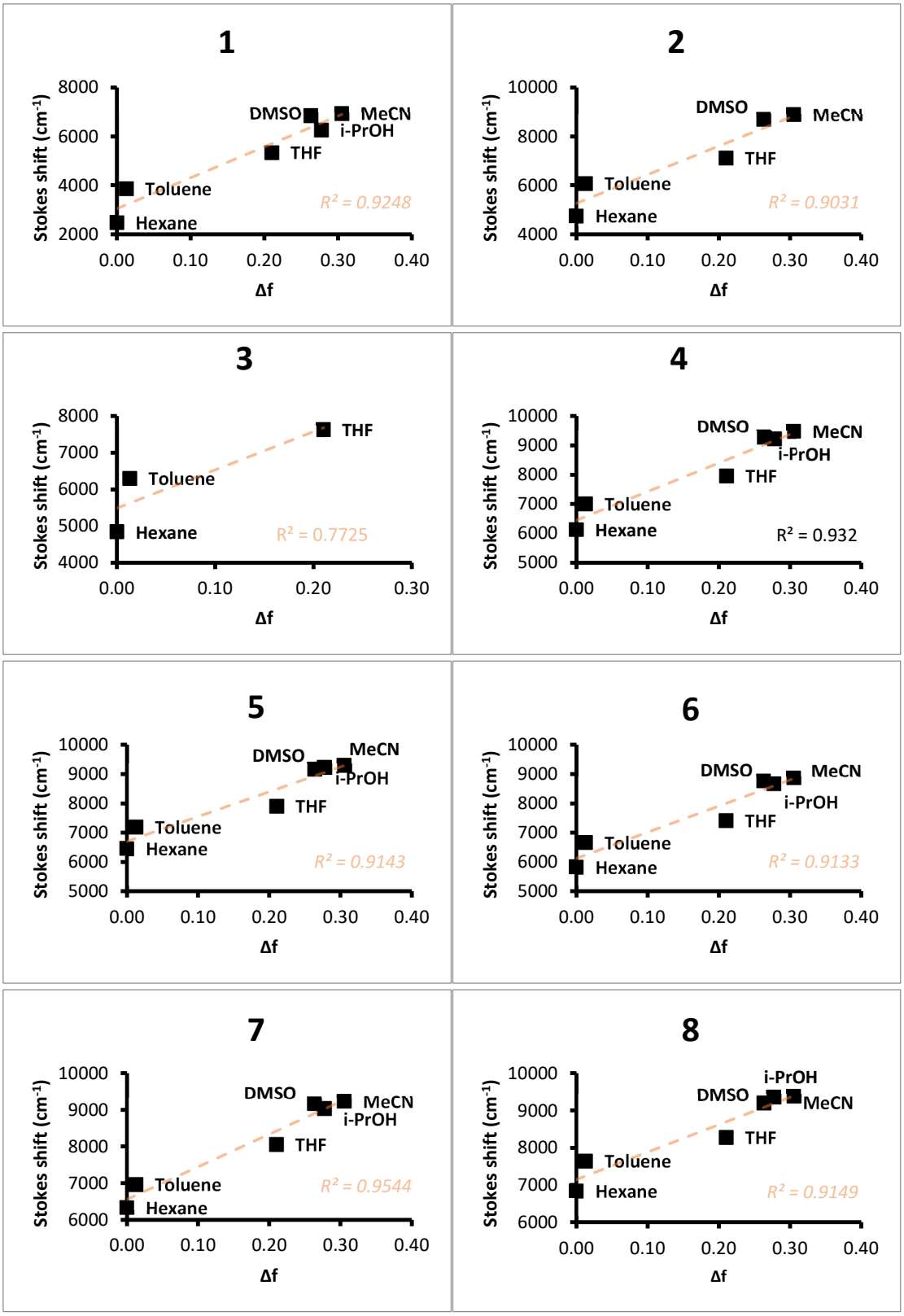

Figure S13: Lippert-Mataga plots of the monosubstituted compounds **1-8**.

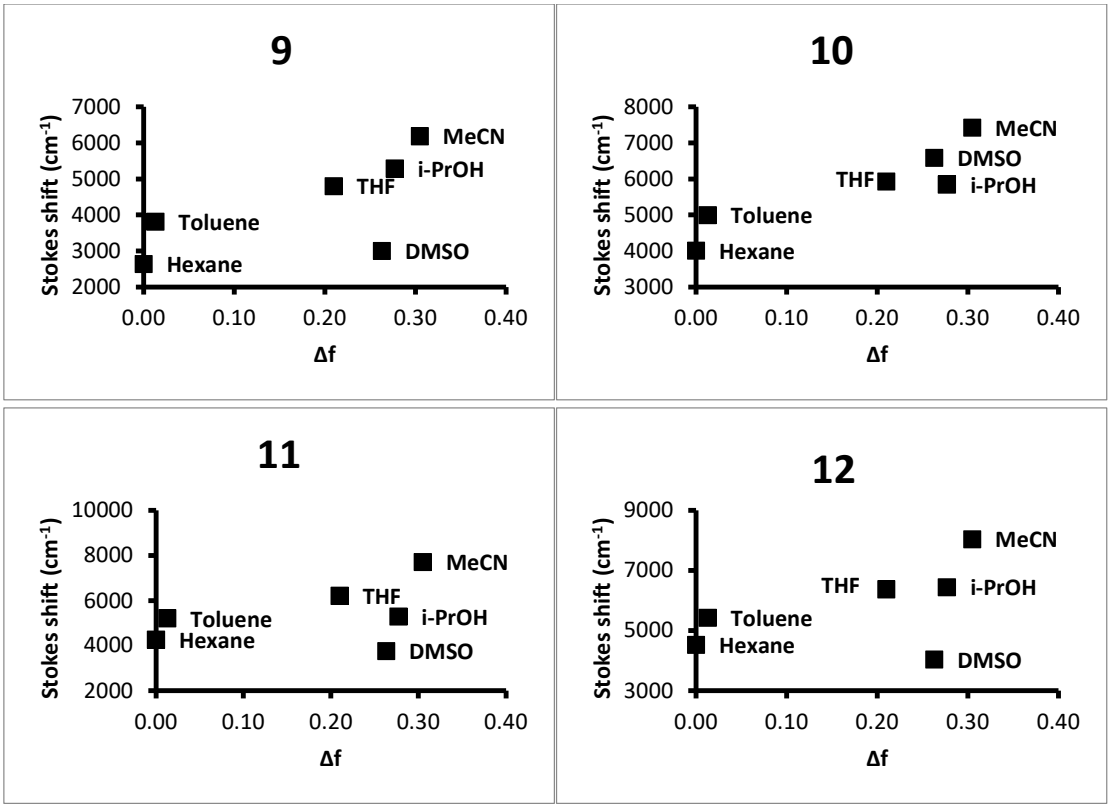

Figure S14: Lippert-Mataga plots of the disubstituted compounds **9-12**. Linear correlations are not shown due to the presence of data points that deviate from the apparent trend.

IV – Additional cell staining images

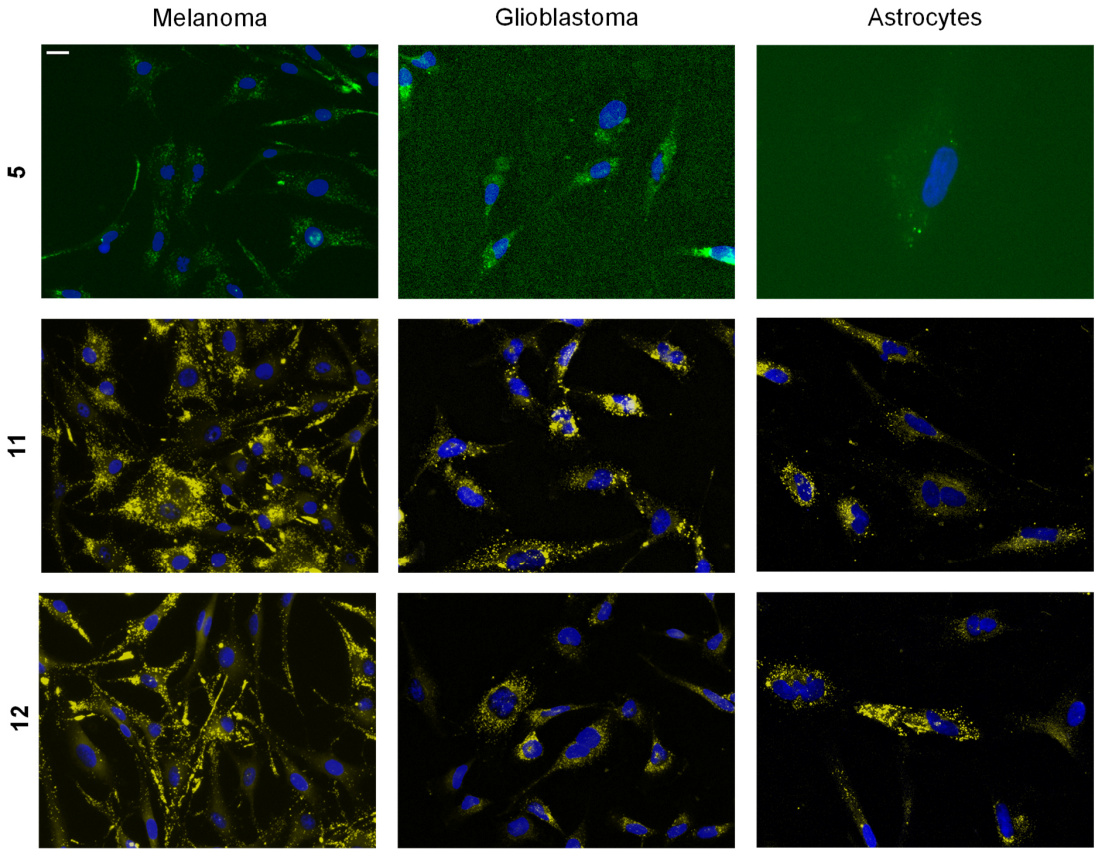

Figure S15: Staining of melanoma (SK-MEL-28, left), glioblastoma (U1242MG, middle) and normal human astrocytes (NHA, right) with **5**, **11** and **12** (10 µM, top and bottom). Staining was performed on live cells, which were fixated after 24 h incubation. Cell nuclei were stained with DAPI (seen in blue). Scale bar: 20 µm.

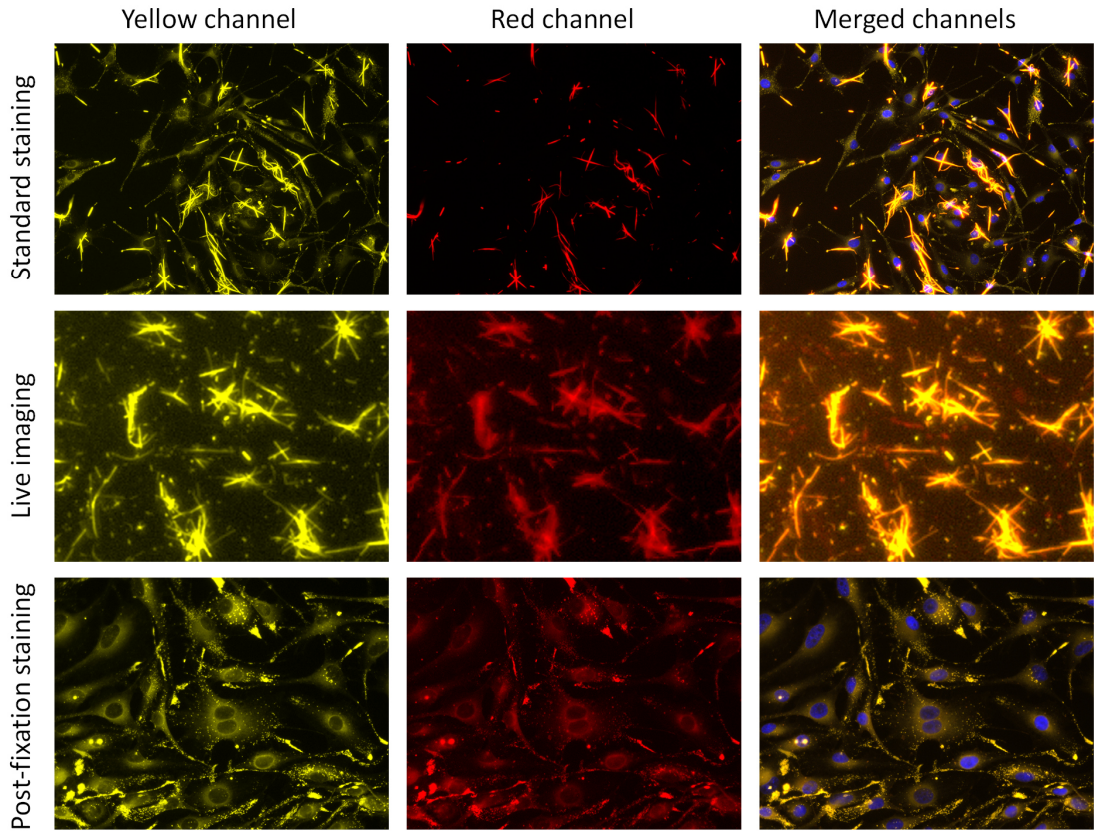

Figure S16: Imaging of melanoma (SK-MEL-28) cells with compound **9** following various staining protocols**.** Top panel: standard protocol used in this study: 10 µM in live cells, 24 h incubation time, then fixation and imaging. Middle panel: 10 µM in live cells, 24 h incubation, then imaging. Bottom panel: cells were fixated, then incubated with 10 µM of the compound for 30 min, then imaging.

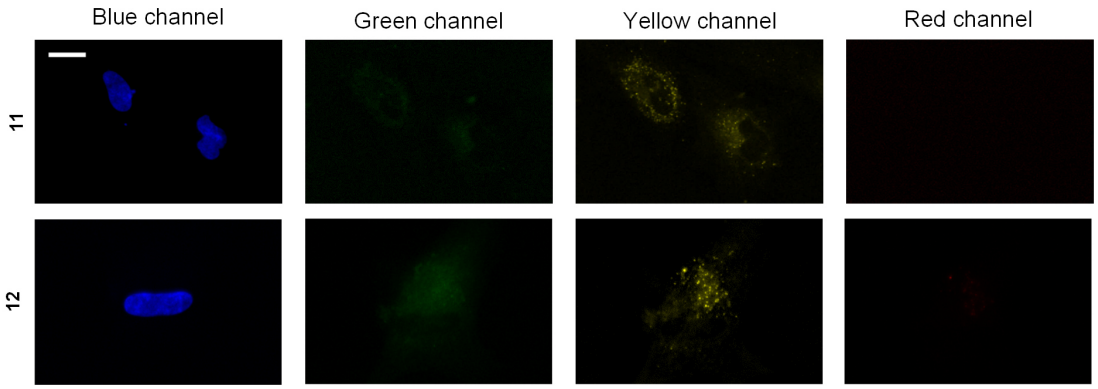

Figure S17: Imaging of normal human astrocytes (NHA) with compounds **11** and **12** (10 µM) in different microscope channels. Blue (Ex 325-375nm, Em 435-485 nm); green (Ex 460-500 nm, Em 512-542 nm); yellow (Ex 532-558 nm, Em 570-640 nm) and red (Ex 590-650nm, Em 662-738nm). Staining was performed on live cells, which were fixated after 24 h incubation. Cell nuclei were stained with DAPI (seen in blue). Scale bar: 20 µm.

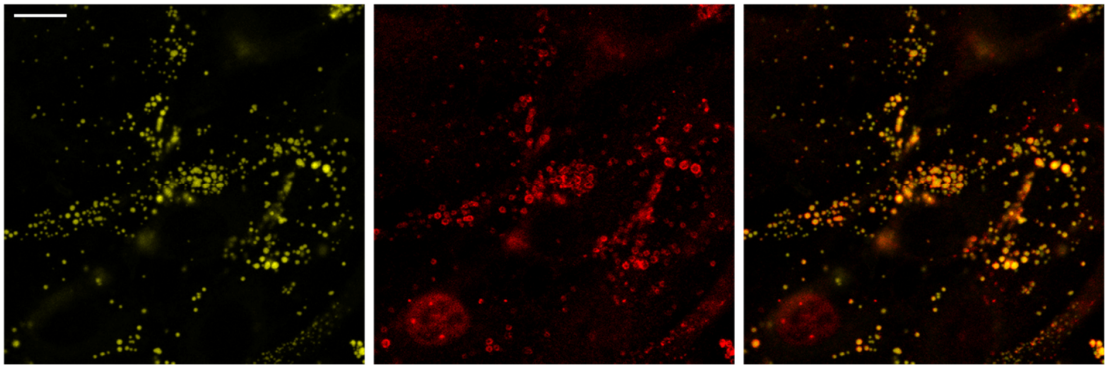

Figure S18: Confocal fluorescence microscopy images of compound **11** (10 µM, 24 h) and the lipid droplet associated protein adipophilin in melanoma cells (SK-MEL-28). Staining was performed on living cells, which were fixated directly after the incubation and further processed for immunofluorescence. Scale bar: 10 µm. The image to the left show compound **11** in yellow (ex 488 nm; em >490 nm), the image in the middle show the anti-adipophilin antibody in red (ex 639 nm; em >600 nm), and the image to the right show merged images to visualize the colocalization of compound **11** and adipophilin.

V – Computational Studies Details

1 - Method

Geometry optimizations without symmetry constraints were carried out with the Gaussian 16 software (revision A.03),[11] using the hybrid M06 functional, with a polarized continuum model (PCM) for the corresponding solvents (*n*-hexane, PhMe, THF, isopropanol, MeOH, MeCN, DMSO and H_2O).[12] The 6-31g*[13-15] basis set is used for all atoms. This combination of functional and basis set has been previously used to investigate structurally similar compounds.[16]

In all cases, optimization yielded structures with singlet ground states (S_0). Frequency calculations were performed at the same level of theory to ensure that the optimized structures were located at a potential energy surface minimum by the absence of imaginary frequencies. Stability calculations were also performed for all optimized structures to ensure that all wavefunctions were stable. Vertical excitation energies were calculated using time-dependent density functional theory (TD-DFT) at the same level of theory with a PCM for the appropriate solvents. In all cases, the vertical excitation transitions are HOMO → LUMO transitions.

2 - Method validation by reproducing reported work: [16]

Table S1: Comparison between **BTD-(OMe)$_2$Ph** modelled in acetonitrile from Ref. [16] and this work. $r_{D\text{-}A}$ is defined as the C-C bond distance that links the two aromatic rings (donor and acceptor) together. $\theta_{D\text{-}A}$ is defined as the torsional angle about the same C-C bond.

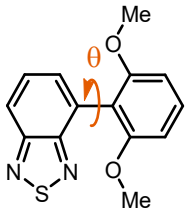

BTD-(OMe)$_2$Ph

Entries	$r_{D\text{-}A}$ (Å)	$\theta_{D\text{-}A}$ (°)	λ (nm)	E (cm^{-1})	*f*	Major contribution to transition
Ref. [16]	1.48	55.4	373	26810	0.12	HOMO → LUMO
This work	1.4823	56.4	372.05	26878	0.1198	HOMO → LUMO

Employing computational details from the methods section, **BTD-(OMe)$_2$Ph** was successfully optimized, yielding a structure with a singlet ground state (S_0). This wavefunction is stable and contains no imaginary frequencies (Lowest frequency: 35.5617 cm^{-1}).

HOMO **LUMO**

Figure S18: HOMO and LUMO surfaces (Isovalue: 0.02) at the optimized S_0 geometries of **BTD-(OMe)$_2$Ph**

Conclusion: Although minor discrepancies were observed in the optimized structure and TD-DFT calculations of **BTD-(OMe)$_2$Ph**, the method used in these calculations yielded results that match well to those found in reference [16].

The frontier orbitals associated with the predicted transitions also match well to those found in Table S16 of Ref. [16], even though a different functional was employed (M06 in this work, B3LYP in report). In addition, computations in different solvents yielded near identical HOMO and LUMO.

3.1 – Calculations for 1 and 9

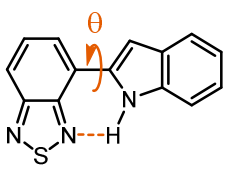

1

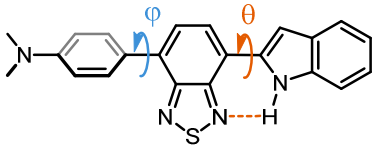

9

Table S2: Compound **1** modelled in various solvents.

Solvent	Lowest frequency (cm^{-1})	r_{In-BTD} (Å)	θ_{In-BTD} (°)	λ (nm)	E (cm^{-1})	*f*
n-hexane	39.4140	1.4523	0.0	507.26	19714	0.2352
PhMe	39.8535	1.4526	0.0	506.23	19754	0.2488
THF	40.0529	1.4534	0.0	494.76	20212	0.2426
^{i}PrOH	39.3243	1.4537	0.0	490.59	20384	0.2410
MeOH	39.0049	1.4538	0.0	488.7	20462	0.2355
MeCN	38.9602	1.4538	0.0	488.85	20456	0.2375
DMSO	38.8421	1.4539	0.0	489.74	20419	0.2460
H_2O	38.6778	1.4539	0.0	487.89	20496	0.2365

Table S3: Compound **9** modelled in various solvents.

Solvent	Lowest frequency (cm^{-1})	r_{In-BTD} (Å)	θ_{In-BTD} (°)	$r_{DMA-BTD}$ (Å)	$\varphi_{DMA-BTD}$ (°)	λ (nm)	E (cm^{-1})	*f*
n-hexane	20.3619	1.4514	0.9	1.4660	31.7	587.96	17008	0.4716
PhMe	20.7012	1.4516	1.0	1.4660	31.8	589.67	16959	0.4922
THF	20.8523	1.4522	1.0	1.4660	32.1	583.68	17133	0.4859
^{i}PrOH	20.9182	1.4525	0.9	1.4661	32.2	581.43	17199	0.4838
MeOH	20.8821	1.4525	0.8	1.4661	32.2	579.78	17248	0.4759
MeCN	20.9153	1.4525	0.8	1.4661	32.2	580.1	17238	0.4788
DMSO	21.0444	1.4526	0.8	1.4661	32.2	581.77	17189	0.4912
H_2O	20.9181	1.4526	0.7	1.4661	32.3	579.49	17257	0.4774

Conclusion: For **1** the HOMO is best described as a π* combination of the BTD and indole fragments, while the LUMO is predominantly BTD-based.
Similar to **1**, the LUMO of **9** is predominantly BTD-based. The HOMO is a π* combination of the BTD and indole fragments, as well as delocalization onto the dimethylaniline (DMA) system. This was also observed in Ref. [16].

3.2 - Effects of *N*-methylation - Calculations for 2 and 10

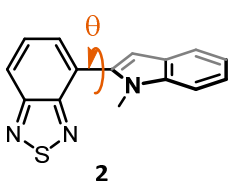

2

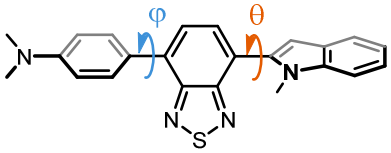

10

Table S4: Compound **2** modelled in various solvents.

Solvent	Lowest frequency (cm^{-1})	$r_{In\text{-}BTD}$ (Å)	$\theta_{In\text{-}BTD}$ (°)	λ (nm)	E (cm^{-1})	*f*
n-hexane	43.9236	1.4609	44.9	477.65	20936	0.1348
PhMe	43.7462	1.4611	45.1	475.87	21014	0.1415
THF	42.3586	1.4617	45.9	465.7	21473	0.1335
^{i}PrOH	41.5062	1.4619	46.3	461.72	21658	0.1304
MeOH	41.2778	1.4620	46.5	460.27	21726	0.1266
MeCN	41.2819	1.4620	46.5	460.24	21728	0.1277
DMSO	41.2330	1.4620	46.5	460.45	21718	0.1323
H_2O	41.1790	1.4620	46.6	459.32	21771	0.1267

Table S5: Compound **10** modelled in various solvents.

Solvent	Lowest frequency (cm^{-1})	$r_{In\text{-}BTD}$ (Å)	$\theta_{In\text{-}BTD}$ (°)	$r_{DMA\text{-}BTD}$ (Å)	$\varphi_{DMA\text{-}BTD}$ (°)	λ (nm)	E (cm^{-1})	*f*
n-hexane	20.3968	1.4603	44.8	1.4673	31.6	533.72	18736	0.4142
PhMe	20.1403	1.4604	45.0	1.4673	31.6	535.63	18670	0.4291
THF	19.2585	1.4609	45.9	1.4674	32.1	534.1	18723	0.4129
^{i}PrOH	18.6856	1.4612	46.4	1.4674	32.4	533.39	18748	0.4053
MeOH	18.5332	1.4612	46.6	1.4674	32.4	532.49	18780	0.3973
MeCN	18.5164	1.4612	46.6	1.4674	32.5	532.73	18771	0.3992
DMSO	18.4590	1.4612	46.6	1.4674	32.5	533.93	18729	0.4083
H_2O	17.8578	1.4606	45.4	1.4669	32.3	532.18	18791	0.4058

Conclusion: The methylated indole compounds **2** and **10** exhibit twisting in the donor and acceptor rings by *ca.* 45° ($\theta_{In\text{-}BTD}$), while their non-methylated counterparts are nearly completely planar ($\theta_{In\text{-}BTD}$ = 0°, see section 3.1).

The predicted vertical excitation energies (**E**) of these methylated analogues are blue shifted and lower in oscillator strength (***f***) in comparison to the compounds lacking methylation. In either case, the predicted transitions originate from HOMOs (π* combination of the BTD and indole/dimethylaniline fragments) and LUMOs (predominantly BTD-based) that are similar in composition.

3.3 - Effects of *N*-isopropyl substitution – Calculations for 3

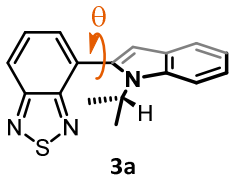

3a

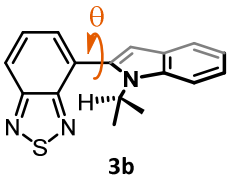

3b

Table S6: Isomer **3a** modelled in various solvents.

Solvent	Lowest frequency (cm^{-1})	$r_{In\text{-}BTD}$ (Å)	$\theta_{In\text{-}BTD}$ (°)	λ (nm)	E (cm^{-1})	*f*
n-hexane	33.4685	1.4687	57.9	475.87	21014	0.0736
PhMe	32.7406	1.4688	58.3	473.07	21139	0.0760
THF	30.4116	1.4694	60.1	461.45	21671	0.0679
^{i}PrOH	31.0566	1.4696	61.0	456.87	21888	0.0643
MeOH	31.1637	1.4697	61.2	455.43	21957	0.0620
MeCN	31.1411	1.4694	61.2	455.33	21962	0.0623
DMSO	31.0643	1.4697	61.4	455.18	21969	0.0643
H_2O	30.8961	1.4697	61.5	454.34	22010	0.0614

Table S7: Isomer **3b** modelled in various solvents.

Solvent	Lowest frequency (cm^{-1})	$r_{In\text{-}BTD}$ (Å)	$\theta_{In\text{-}BTD}$ (°)	λ (nm)	E (cm^{-1})	*f*
n-hexane	32.5775	1.4642	48.1	478.42	20902	0.1083
PhMe	32.2296	1.4644	48.3	476.02	21008	0.1136
THF	32.6952	1.4651	49.6	464.34	21536	0.1045
^{i}PrOH	32.7045	1.4654	50.2	459.6	21758	0.1013
MeOH	32.6060	1.4655	50.3	458	21834	0.0982
MeCN	32.5886	1.4655	50.3	457.93	21837	0.0989
DMSO	32.5406	1.4655	50.4	457.93	21837	0.1026
H_2O	32.4753	1.4655	50.5	456.88	21888	0.0980

Conclusion: The isopropylated compound **3** is predicted to exist as two isomers **3a** and **3b**. Compared to the methylated compound **2**, **3a** and **3b** display sharply increased torsion angles ($\theta_{In\text{-}BTD}$) of *ca*. 60° and 50°, respectively, which are the largest in the series. The predicted vertical excitation energies are virtually identical to those of the methylated analogue **2**. Isomer **3b** is predicted to be 2.0 kcal/mol lower in energy than **3a** in all solvent models. The predicted transitions originate from HOMOs (π* combination of the BTD and indole fragments) and LUMOs (predominantly BTD-based) that are similar in composition.

3.3 - Effect of *N*-acylation - Calculations for 4 and 11

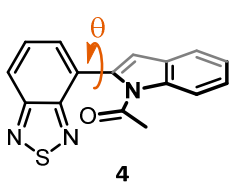

4

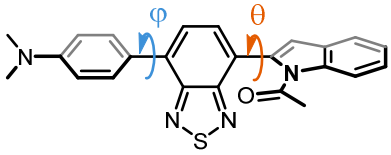

11

Table S8: Compound **4** modelled in various solvents.

Solvent	Lowest frequency (cm^{-1})	$r_{In\text{-}BTD}$ (Å)	$\theta_{In\text{-}BTD}$ (°)	λ (nm)	E (cm^{-1})	*f*
n-hexane	26.0795	1.4611	47.0	407.73	24526	0.1887
PhMe	25.3710	1.4613	47.1	408.84	24459	0.1978
THF	15.9777	1.4618	47.6	409.13	24442	0.1834
^{i}PrOH	18.9881	1.4621	48.0	408.91	24455	0.1781
MeOH	19.6471	1.4621	48.1	408.72	24467	0.1729
MeCN	19.7268	1.4621	48.1	408.86	24458	0.1743
DMSO	19.9246	1.4622	48.1	409.46	24422	0.1804
H_2O	20.1738	1.4622	48.1	408.93	24454	0.1727

Table S9: Compound **11** modelled in various solvents.

Solvent	Lowest frequency (cm^{-1})	$r_{In\text{-}BTD}$ (Å)	$\theta_{In\text{-}BTD}$ (°)	$r_{DMA\text{-}BTD}$ (Å)	$\varphi_{DMA\text{-}BTD}$ (°)	λ (nm)	E (cm^{-1})	*f*
n-hexane	17.5314	1.4589	45.0	1.4673	32.2	511.48	19551	0.4147
PhMe	15.5658	1.4591	45.2	1.4673	32.2	514.89	19422	0.4260
THF	16.1130	1.4597	45.9	1.4673	32.4	519.49	19250	0.4006
^{i}PrOH	16.9643	1.4599	46.1	1.4674	32.5	521.52	19175	0.3916
MeOH	17.1283	1.4600	46.2	1.4674	32.6	521.39	19180	0.3834
MeCN	17.1224	1.4600	46.2	1.4674	32.6	521.77	19166	0.3854
DMSO	17.1893	1.4600	46.2	1.4674	32.6	523.12	19116	0.3943
H_2O	17.2447	1.4600	46.2	1.4674	32.6	522.08	19154	0.3828

Conclusion: The acetylated (**4, 11**) vs. methylated compounds (**2, 10**) exhibited near-identical metrical parameters ($r_{In\text{-}BTD}$, $\theta_{In\text{-}BTD}$).

The predicted vertical excitation energies (**E**) of these acetylated analogues are blue shifted in comparison to the methylated compounds. In all cases, the predicted transitions originate from HOMOs (π* combination of the BTD and indole/dimethylaniline fragments) and LUMOs (predominantly BTD-based) that are similar in composition, with minimal contribution from the acetyl groups.

3.4 - Effect of *N*-benzoyl and *N*-Boc substitution – Calculations for 5, 6 and 12

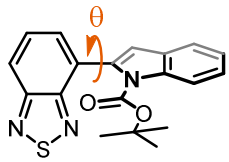

5

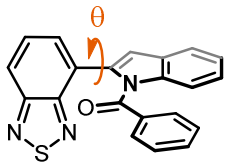

6

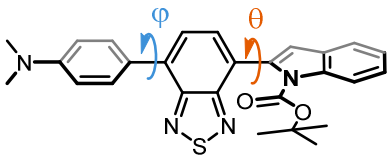

12

Table S10: Compound **5** modelled in various solvents.

Solvent	Lowest frequency (cm^{-1})	$r_{In\text{-}BTD}$ (Å)	$\theta_{In\text{-}BTD}$ (°)	λ (nm)	E (cm^{-1})	*f*
n-hexane	25.7913	1.4608	46.0	416.46	24012	0.1894
PhMe	18.8878	1.4606	45.5	418.78	23879	0.1995
THF	18.1413	1.4604	44.6	419.79	23821	0.1900
*i*PrOH	18.8551	1.4602	44.2	420.53	23780	0.1866
MeOH	19.8422	1.4603	44.2	420.24	23796	0.1814
MeCN	19.8341	1.4603	44.2	420.39	23787	0.1829
DMSO	19.9803	1.4603	44.1	421.06	23750	0.1897
H2O	20.1250	1.4603	44.1	420.44	23785	0.1817

Table S11: Compound **6** modelled in various solvents.

Solvent	Lowest frequency (cm^{-1})	$r_{In\text{-}BTD}$ (Å)	$\theta_{In\text{-}BTD}$ (°)	λ (nm)	E (cm^{-1})	*f*
n-hexane	28.6966	1.4588	41.7	423.47	23614	0.1846
PhMe	28.9453	1.4589	41.7	424.14	23577	0.1945
THF	29.2376	1.4594	41.8	423.01	23640	0.1839
^{i}PrOH	29.1687	1.4595	41.9	422.83	23650	0.1799
MeOH	29.1552	1.4596	41.9	422.5	23669	0.1749
MeCN	29.1505	1.4596	41.9	422.64	23661	0.1763
DMSO	29.1381	1.4595	41.9	423.24	23627	0.1827
H_2O	29.1208	1.4596	42.0	422.59	23664	0.1749

Table S12: Compound **12** modelled in various solvents.

Solvent	Lowest frequency (cm^{-1})	$r_{In\text{-}BTD}$ (Å)	$\theta_{In\text{-}BTD}$ (°)	$r_{DMA\text{-}BTD}$ (Å)	$\varphi_{DMA\text{-}BTD}$ (°)	λ (nm)	E (cm^{-1})	*f*
n-hexane	16.8191	1.4591	45.1	1.4675	31.5	509.52	19626	0.4291
PhMe	16.1529	1.4591	44.9	1.4675	31.6	513.65	19469	0.4412
THF	15.5445	1.4584	42.9	1.4672	32.2	524.27	19074	0.4226
^{i}PrOH	17.1866	1.4584	42.5	1.4672	32.3	526.88	18980	0.4157
MeOH	16.2517	1.4584	42.5	1.4671	32.4	527.5	18957	0.4073
MeCN	16.2746	1.4584	42.4	1.4671	32.4	527.91	18943	0.4095
DMSO	16.3174	1.4584	42.4	1.4671	32.4	529.44	18888	0.4192
H_2O	16.3541	1.4584	42.4	1.4671	32.4	528.45	18923	0.4070

Conclusion: The benzoyl-substituted (**6**) and Boc-substituted (**5, 12**) compounds exhibited similar $r_{In\text{-}BTD}$ (*ca.* 1.46 Å) to their acetylated counterpart (**4, 11**). The torsional angle between the rings ($\theta_{In\text{-}BTD}$) increased from **6** to **5**/**12** to **4**.

The predicted vertical excitation energies (E) blue-shifts from **12** to **5**/**6** to **4**. In all cases, the predicted transitions originate from HOMOs (π* combination of the BTD and indole/dimethylaniline fragments) and LUMOs (predominantly BTD-based) that are similar in composition, with minimal contribution from the carbonyl groups.

3.6 - Effects of larger *N*-substitution – Calculations for 7 and 8

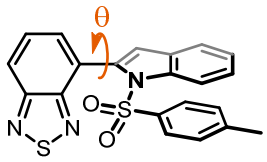

7

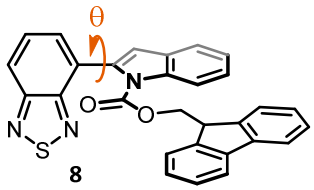

8

Table S13: Compound **7** modelled in various solvents.

Solvent	Lowest frequency (cm^{-1})	r_{In-BTD} (Å)	θ_{In-BTD} (°)	λ (nm)	E (cm^{-1})	*f*
n-hexane	17.3240	1.4617	49.8	392.36	25487	0.2137
PhMe	17.7937	1.4617	49.7	393.79	25394	0.2239
THF	17.8224	1.4619	49.6	395.39	25291	0.2066
^{i}PrOH	17.0317	1.4620	49.6	396.14	25244	0.2
MeOH	17.0900	1.4620	49.6	396.05	25249	0.1937
MeCN	17.0698	1.4621	49.6	396.21	25239	0.1954
DMSO	17.1273	1.4621	49.6	396.83	25200	0.2019
H_2O	15.7978	1.4620	49.6	396.41	25226	0.1932

Table S14: Compound **8** modelled in various solvents.

Solvent	Lowest frequency (cm^{-1})	r_{In-BTD} (Å)	θ_{In-BTD} (°)	λ (nm)	E (cm^{-1})	*f*
n-hexane	17.0335	1.4623	49.7	402.2	24863	0.1839
PhMe	17.3593	1.4624	49.8	403.17	24803	0.1923
THF	17.8595	1.4627	50.2	403.28	24797	0.1780
^{i}PrOH	17.6029	1.4628	50.3	403.45	24786	0.1735
MeOH	17.4638	1.4628	50.3	403.21	24801	0.1685
MeCN	17.4435	1.4628	50.3	403.34	24793	0.1699
DMSO	17.3891	1.4628	50.3	403.88	24760	0.1761
H_2O	17.3111	1.4628	50.3	403.35	24792	0.1685

Conclusion: The tosyl- (**7**) and Fmoc-substituted (**8**) compounds exhibited similar r_{In-BTD} (*ca.* 1.46 Å) to counterparts bearing acyl protecting groups (**4-6, 11-12**). In both cases the torsional angle between the rings (θ_{In-BTD}) increased sharply to *ca*. 50°.

The predicted vertical excitation energies (E) are similar to the above-mentioned derivatives, with a noticeable blue-shift for tosylated compound **7**. In all cases, the predicted transitions originate from HOMOs (π* combination of the BTD and indole/dimethylaniline fragments) and LUMOs (predominantly BTD-based) that are similar in composition.

VI – References

1. Fulmer, G. R.; Miller, A. J. M.; Sherden, N. H.; Gottlieb, H. E.; Nudelman, A.; Stoltz, B. M.; Bercaw, J. E.; Goldberg, K. I. *Organometallics* **2010**, *29*, 2176.

2. Sjöback, R.; Nygren, J.; Kubista, M. *Spectrochim. Acta Part A.* **1995**, *51*, L7.

3. Brouwer, A. M. *Pure Appl. Chem.* **2011**, *83*, 2213.

4. Kozma, I. Z.; Krok, P.; Riedle, E. *J. Opt. Soc. Am. B* **2005**, *22*, 1479.

5. Moutzouris, K.; Papamichael, M.; Betsis, S. C.; Stavrakas, I.; Hloupis, G.; Triantis, D. *Appl. Phys. B.* **2014**, *116*, 617.

6. Kedenburg, S.; Vieweg, M.; Gissibl, T.; Giessen, H. *Opt. Mater. Express* **2012**, *2*, 1588.

7. H. Liu, L. Wang, M. Lv, R. Pei, P. Li, Z. Pei, Y. Wang, W. Su, X.-Q. Xie, *J. Chem. Inf. Model.,* **2014**, *54*, 1050-1060.

8. Appelqvist, H.; Stranius, K.; Börjesson, K.; Nilsson, K. P. R.; Dyrager, C. *Bioconjugate Chem.* **2017**, *28*, 1363.

9. Ito, S.; Yamada, T.; Taguchi, T.; Yamaguchi, Y.; Asami, M. *Chem. Asian J.* **2016**, *11*, 1963.

10. Kato, S.-i.; Matsumoto, T.; Shigeiwa, M.; Gorohmaru, H.; Maeda, S.; Ishi-i, T.; Mataka, S. *Chem. Eur. J.* **2006**, *12*, 2303.

11. Frisch, M. J.; Trucks, G. W.; Schlegel, H. B.; Scuseria, G. E.; Robb, M. A.; Cheeseman, J. R.; Scalmani, G.; Barone, V.; Mennucci, B.; Petersson, G. A.; Nakatsuji, H.; Caricato, M.; Li, X.; Hratchian, H. P.; Izmaylov, A. F.; Bloino, J.; Zheng, G.; Sonnenberg, J. L.; Hada, M.; Ehara, M.; Toyota, K.; Fukuda, R.; Hasegawa, J.; Ishida, M.; Nakajima, T.; Honda, Y.; Kitao, O.; Nakai, H.; Vreven, T.; Montgomery, J. A., Jr.; Peralta, J. E.; Ogliaro, F.; Bearpark, M.; Heyd, J. J.; Brothers, E.; Kudin, K. N.; Staroverov, V. N.; Kobayashi, R.; Normand, J.; Raghavachari, K.; Rendell, A.; Burant, J. C.; Iyengar, S. S.; Tomasi, J.; Cossi, M.; Rega, N.; Millam, J. M.; Klene, M.; Knox, J. E.; Cross, J. B.; Bakken, V.; Adamo, C.; Jaramillo, J.; Gomperts, R.; Stratmann, R. E.; Yazyev, O.; Austin, A. J.; Cammi, R.; Pomelli, C.; Ochterski, J. W.; Martin, R. L.; Morokuma, K.; Zakrzewski, V. G.; Voth, G. A.; Salvador, P.; Dannenberg, J. J.; Dapprich, S.; Daniels, A. D.; Farkas, Ö.; Foresman, J. B.; V.Ortiz, J.; Cioslowski, J.; Fox, D. J. Gaussian 16, revision A.03; Gaussian, Inc.: Wallingford, CT, 2009

12. Cossi, M.; Scalmani, G.; Rega, N.; Barone, V. *J. Chem. Phys.*, **2002**, *117*, 43

13. Petersson, G. A.; Al-Laham, M. A. *J. Chem. Phys.*, **1991**, *94*, 6081.

14. Francl, M. M.; Petro, W. J.; Hehre, W. J.; Binkley, J. S.; Gordon, M. S.; DeFree, D. J.; Pople, J. A. *J. Chem. Phys.*, **1982**, *77*, 3654.

15. Hariharan, P. C.; Pople, J. A. *Theor. Chim. Acta* **1973**, *28*, 213.

16. Barnsley, J. E., Shillito, G. E., Larsen, C. B., van der Salm, H., Wang, L. E., Lucas, N. T., Gordon, K. C. *J. Phys. Chem. A*, **2016**, *120*, 1853 – 1866.

VII – NMR spectra of new compounds

*^{1}H NMR (400 MHz, $CDCl_3$) of compound **2***

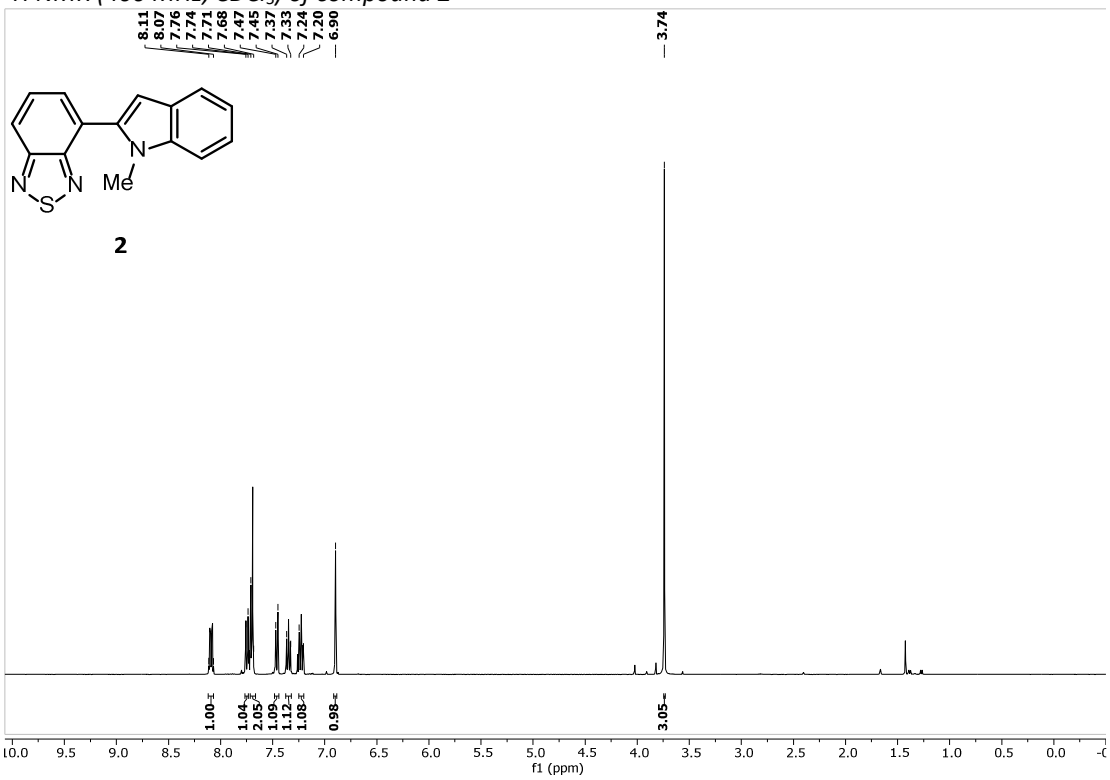

*^{13}C NMR (101 MHz, $CDCl_3$) of compound **2***

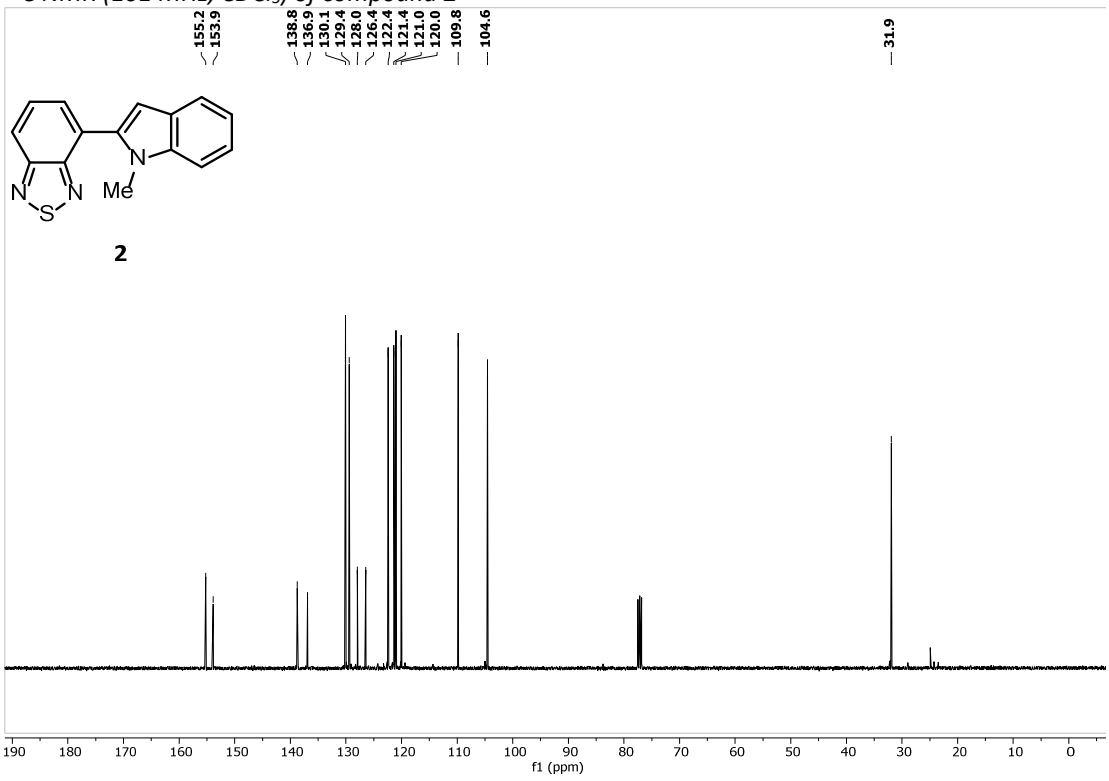

*^{1}H NMR (400 MHz, $CDCl_3$) of compound **3***

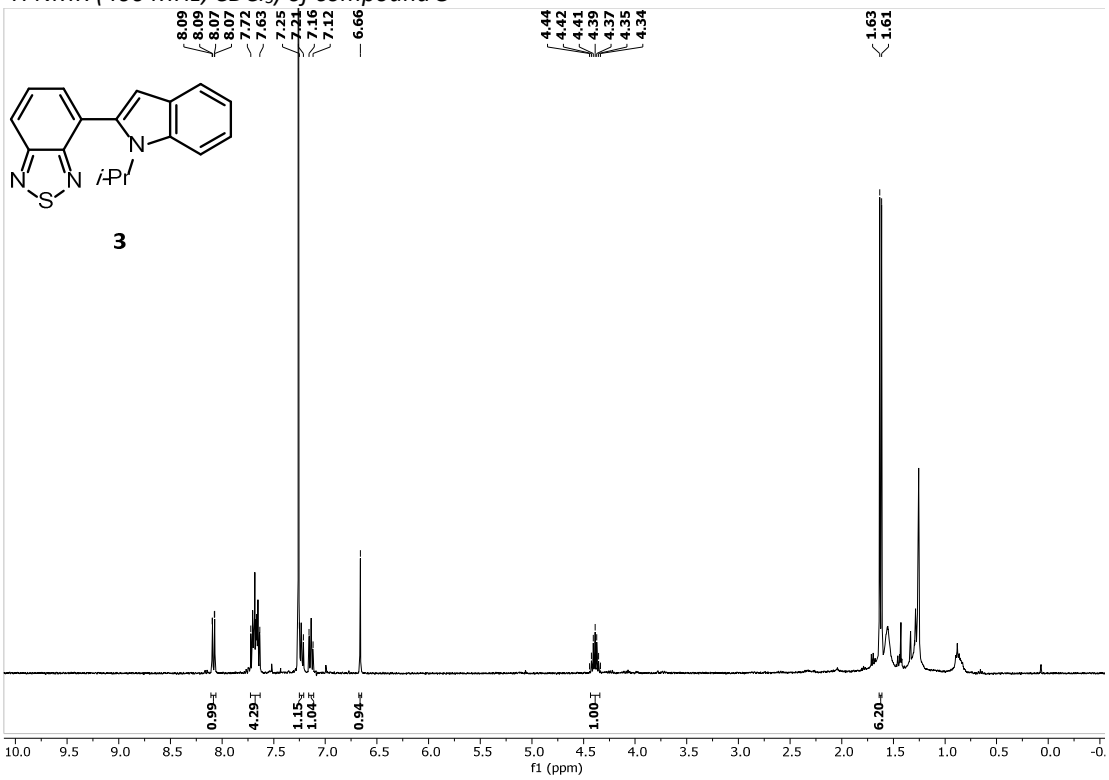

*^{13}C NMR (101 MHz, $CDCl_3$) of compound **3***

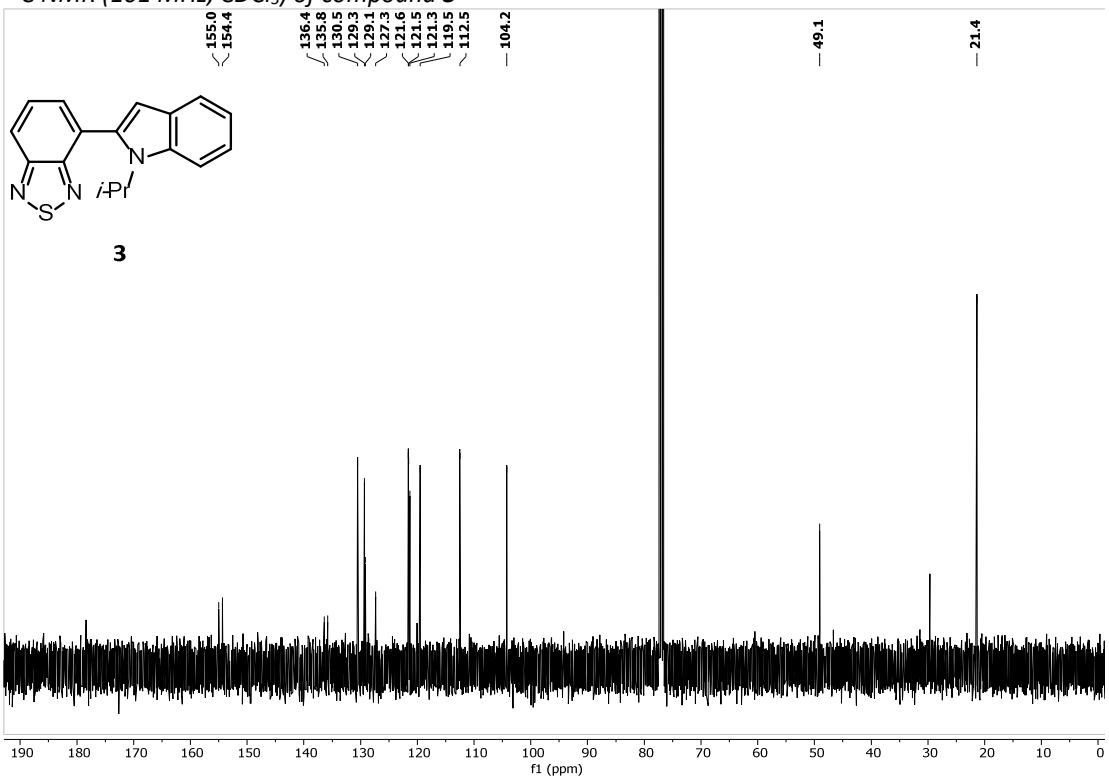

*^{1}H NMR (400 MHz, $CDCl_3$) of compound **4***

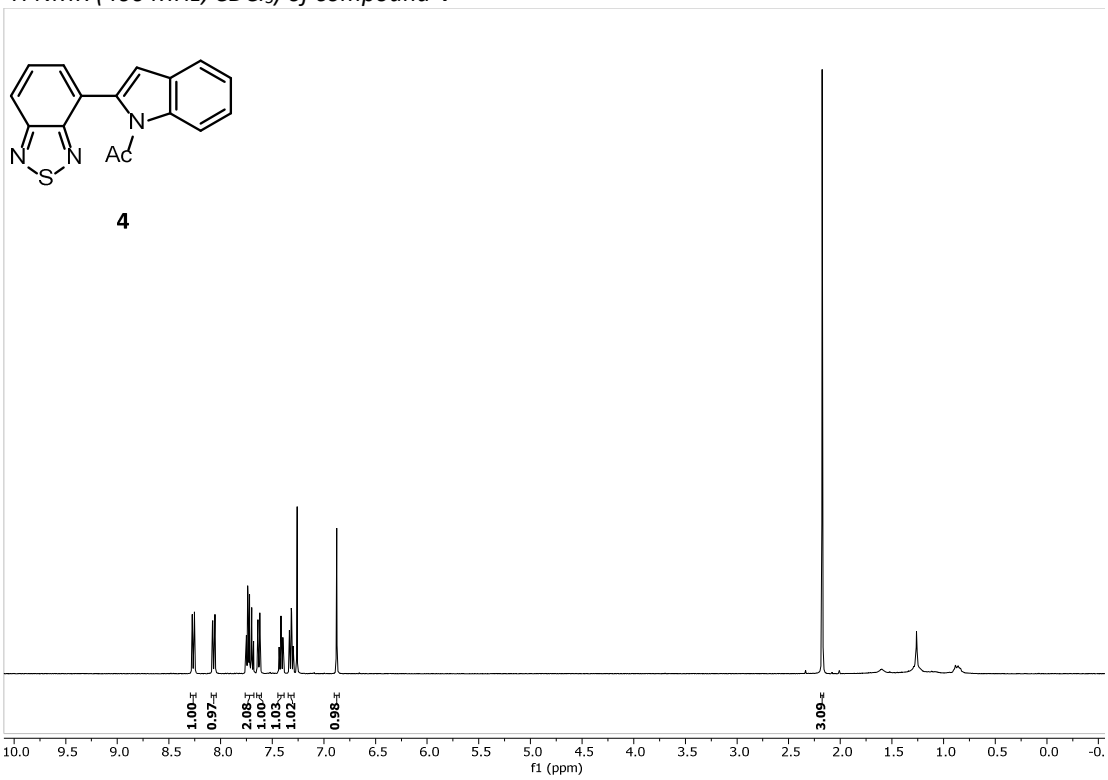

*^{13}C NMR (101 MHz, $CDCl_3$) of compound **4***

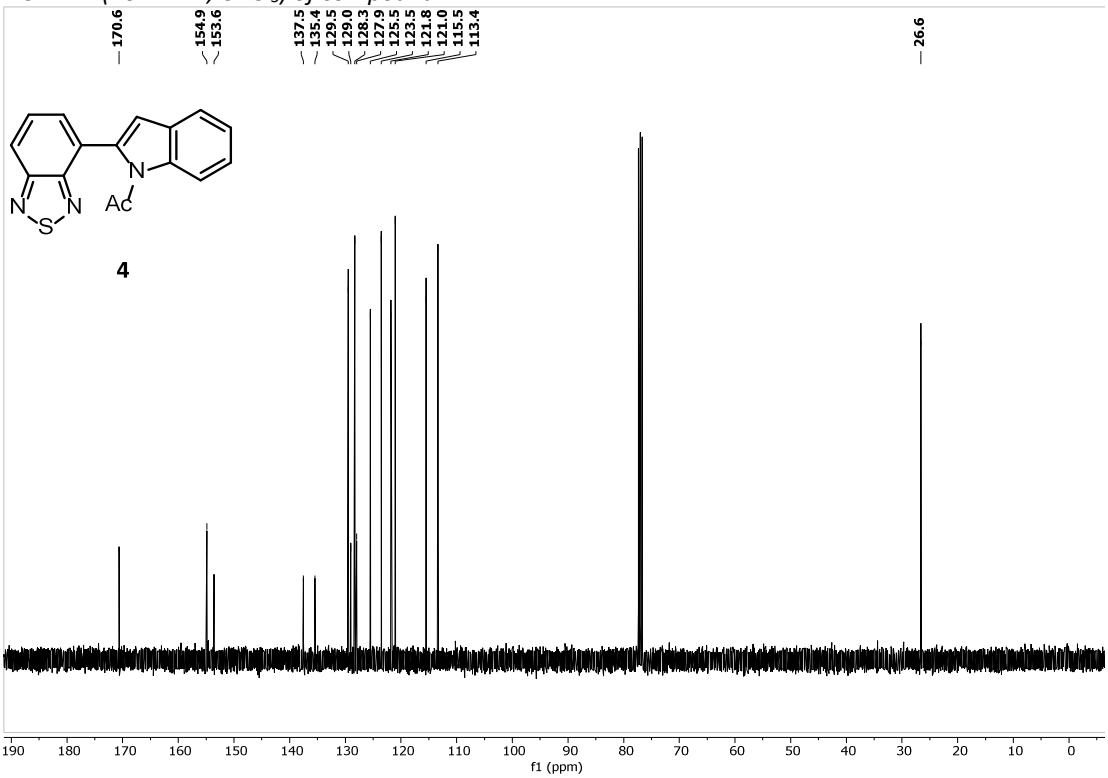

*^{1}H NMR (400 MHz, $CDCl_3$) of compound **6***

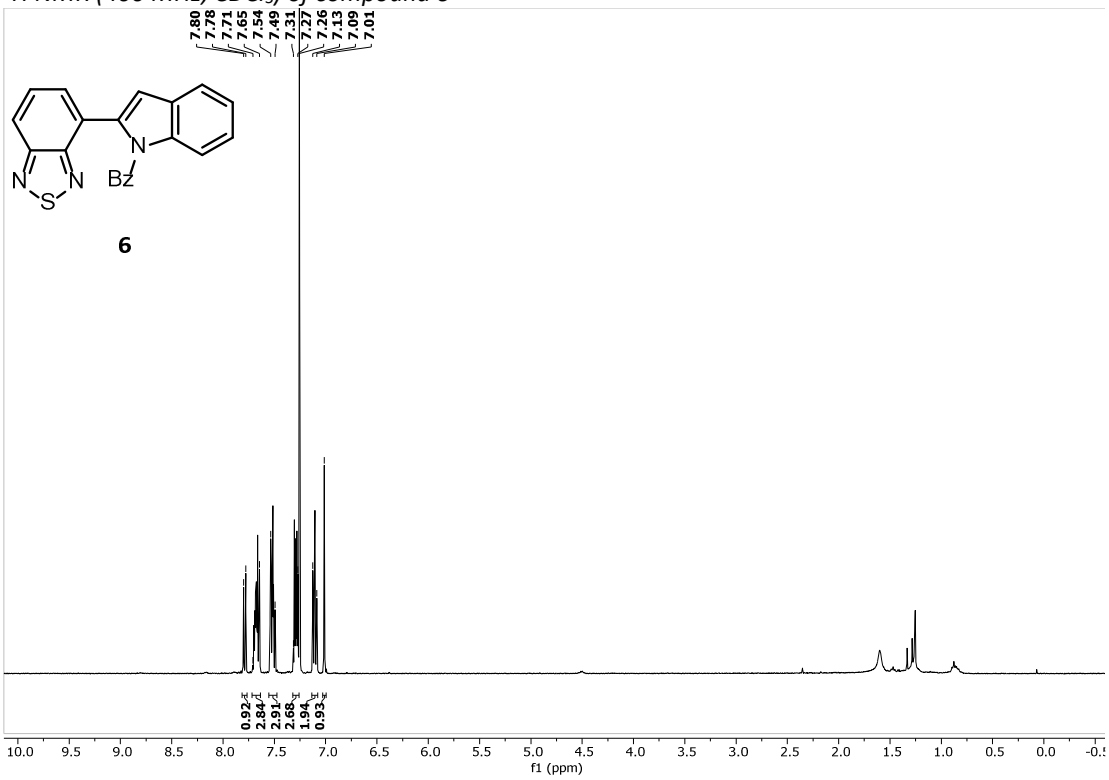

*^{13}C NMR (101 MHz, $CDCl_3$) of compound **6***

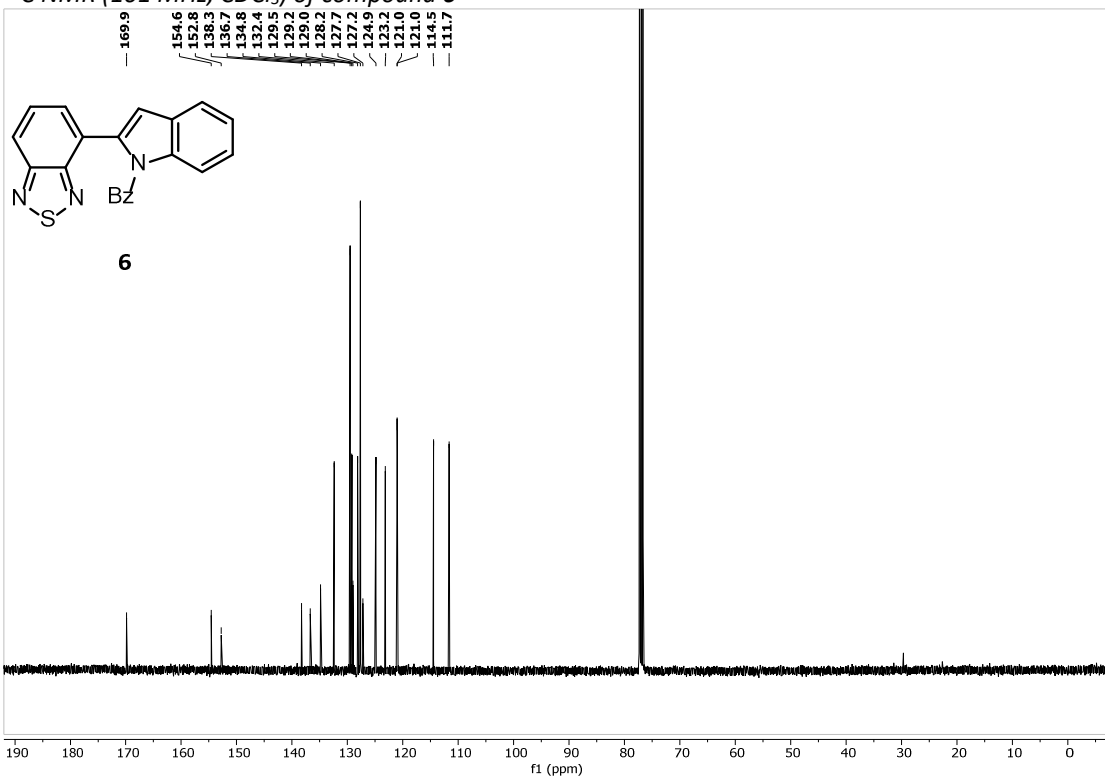

*^{1}H NMR (400 MHz, $CDCl_3$) of compound **7***

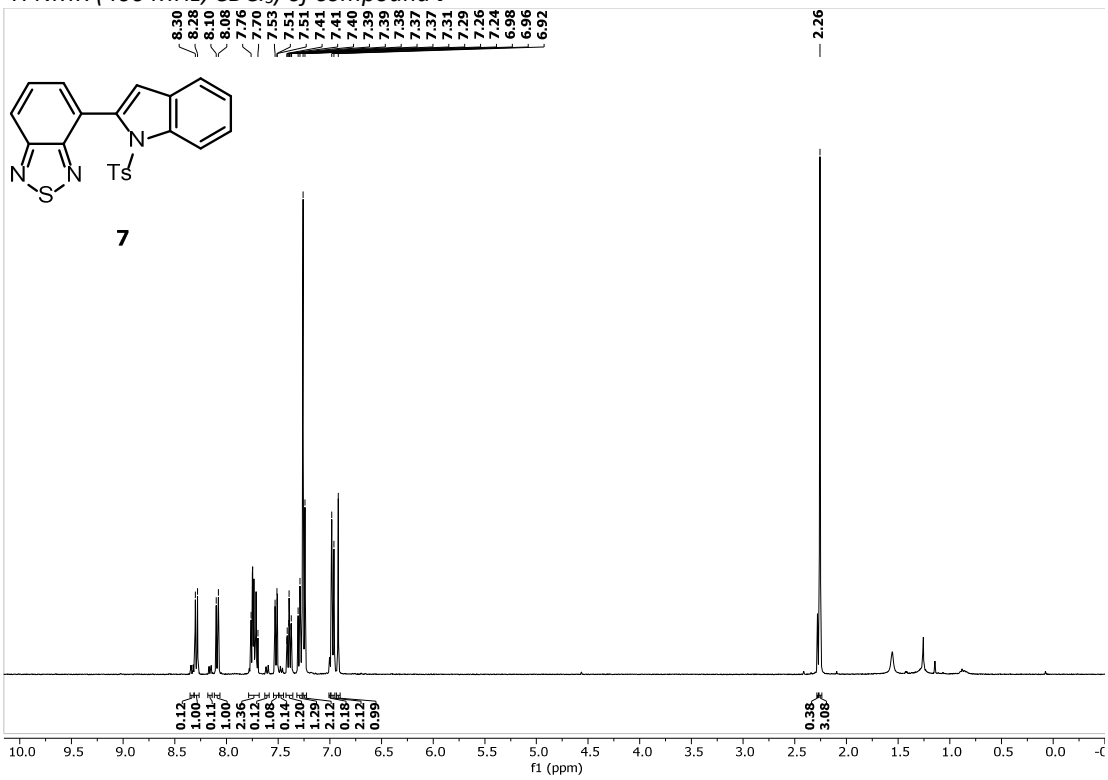

*^{13}C NMR (101 MHz, $CDCl_3$) of compound **7***

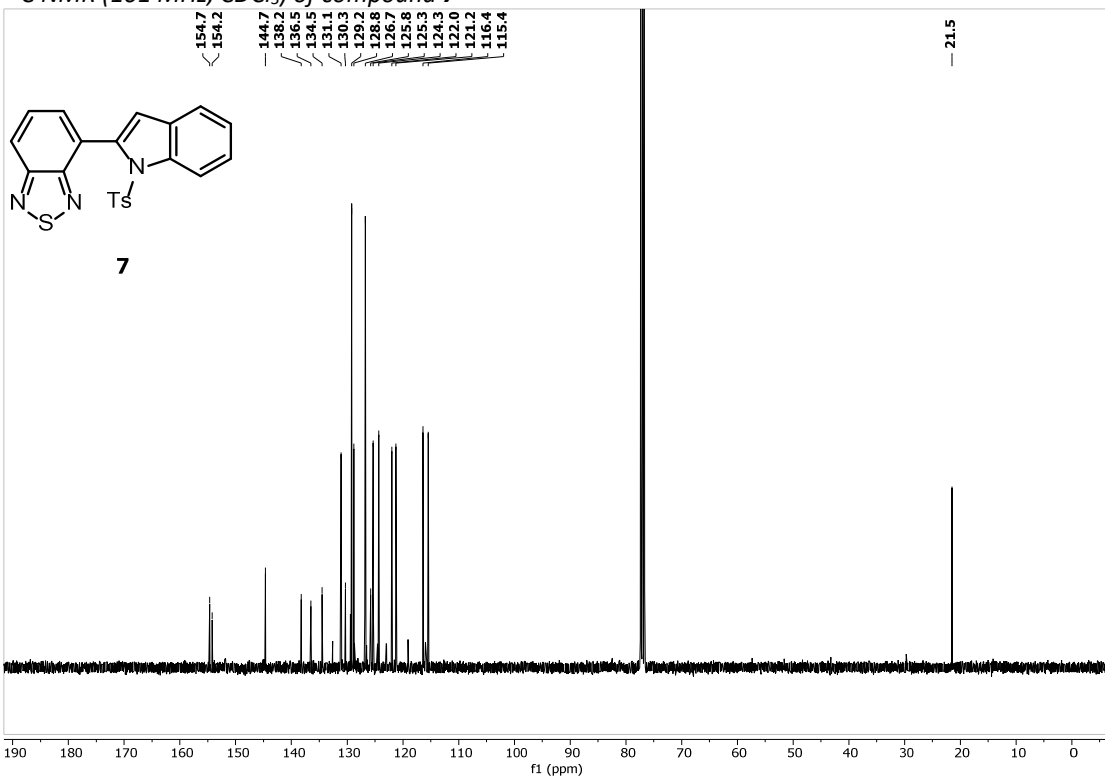

*^{1}H NMR (400 MHz, $CDCl_3$) of compound **8***

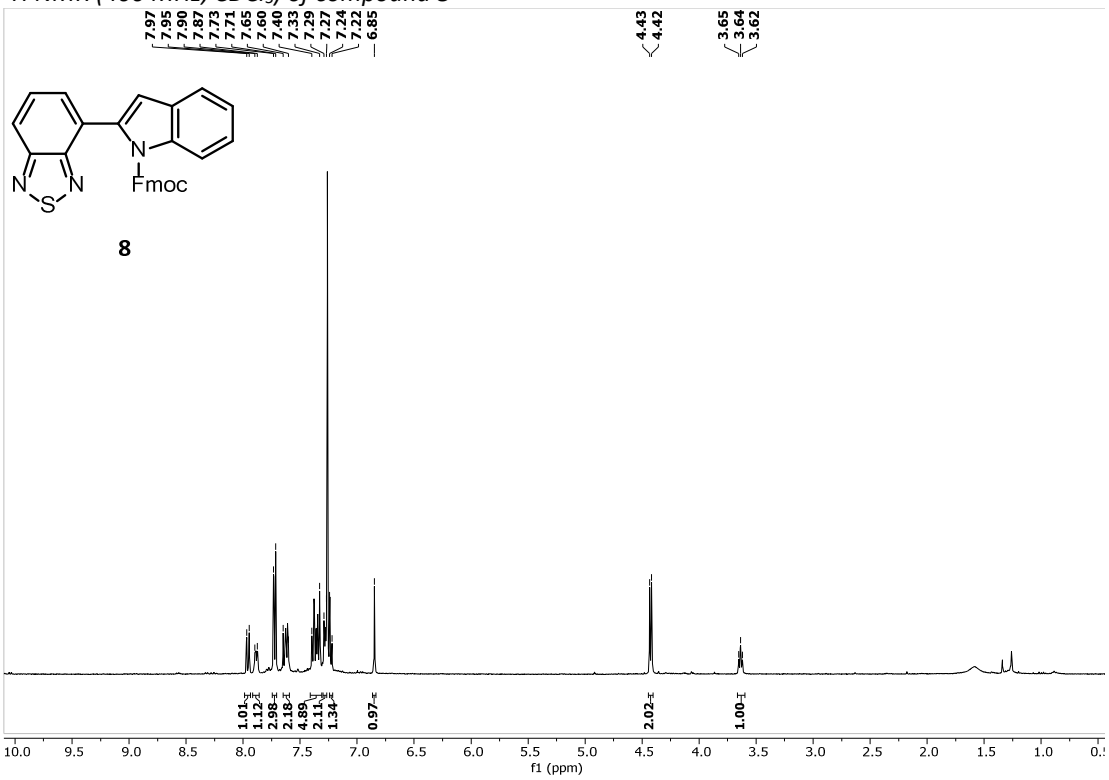

*^{13}C NMR (101 MHz, $CDCl_3$) of compound **8***

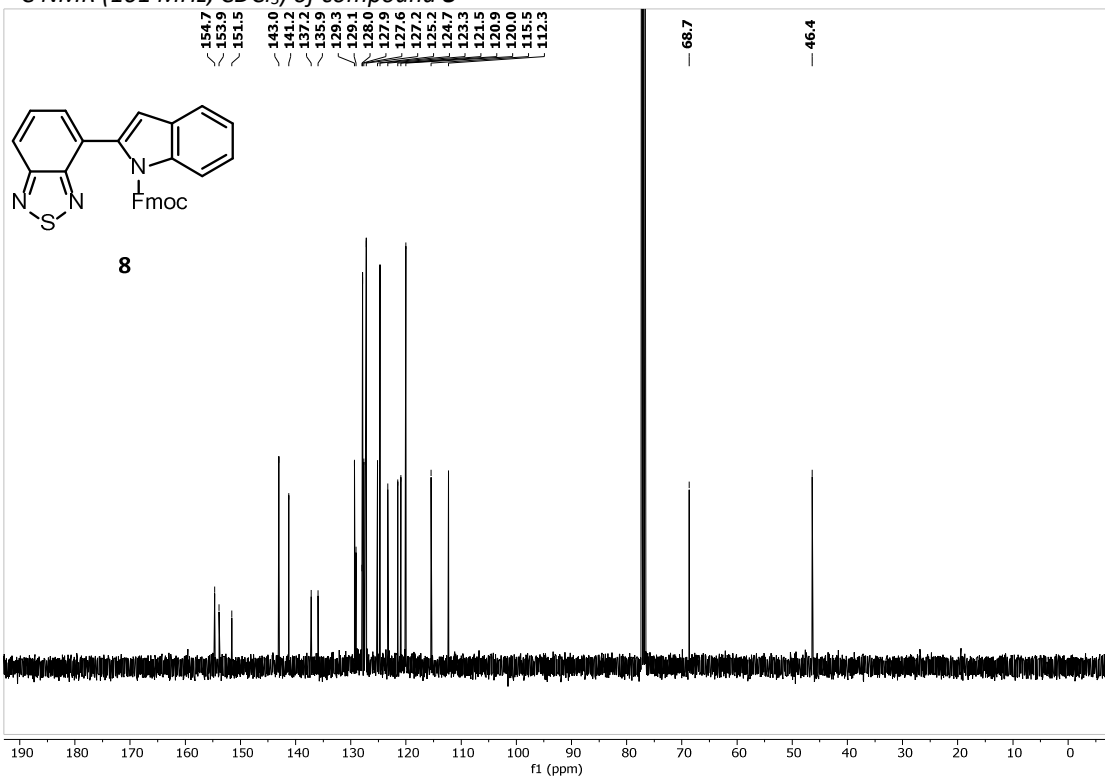

*^{1}H NMR (400 MHz, $CDCl_3$) of compound **9***

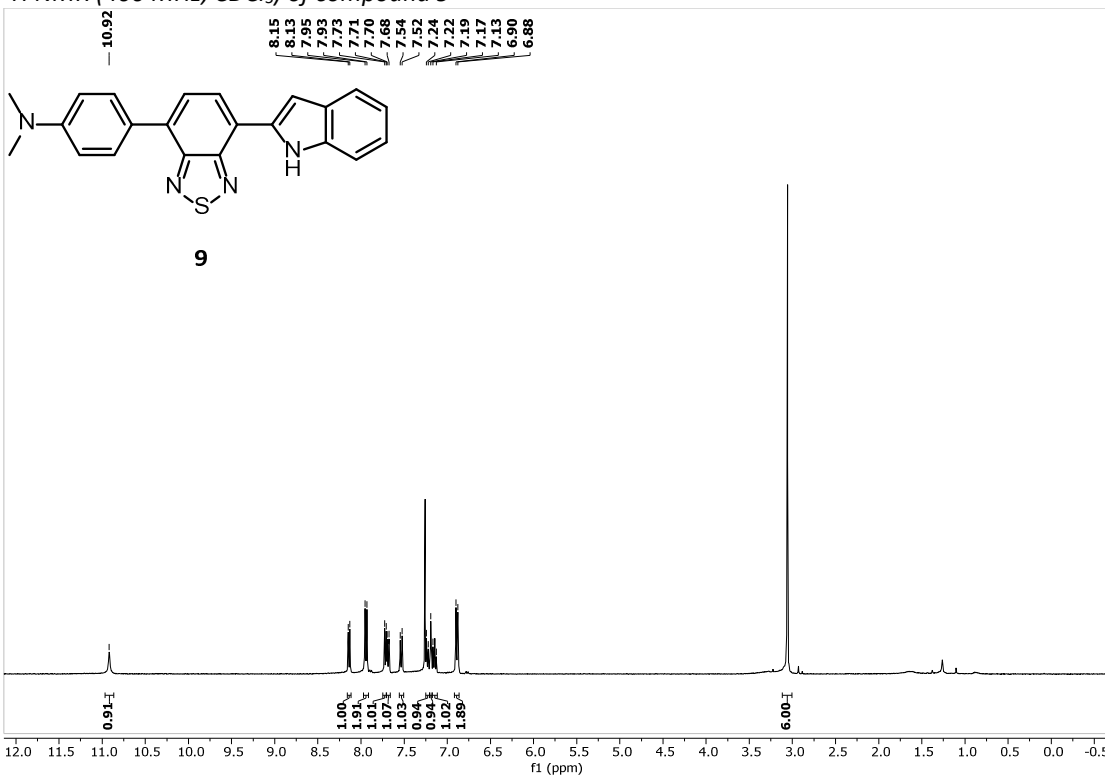

*^{13}C NMR (101 MHz, $CDCl_3$) of compound **9***

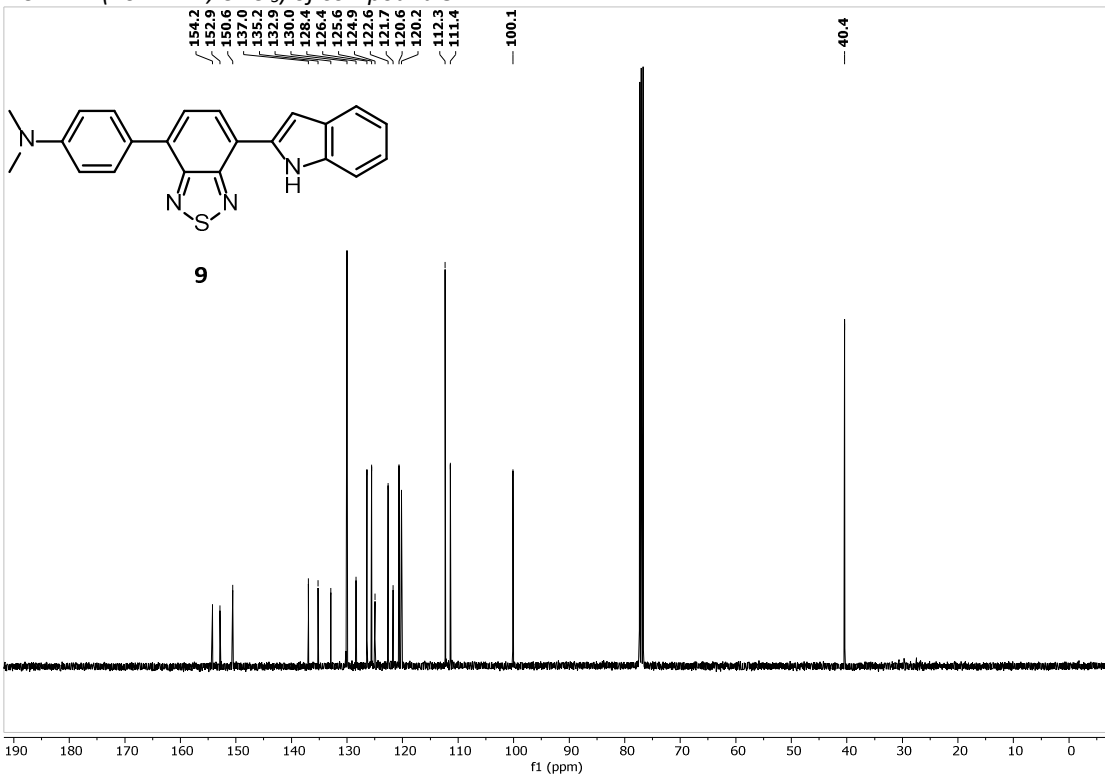

*^{1}H NMR (400 MHz, $CDCl_3$) of compound **10***

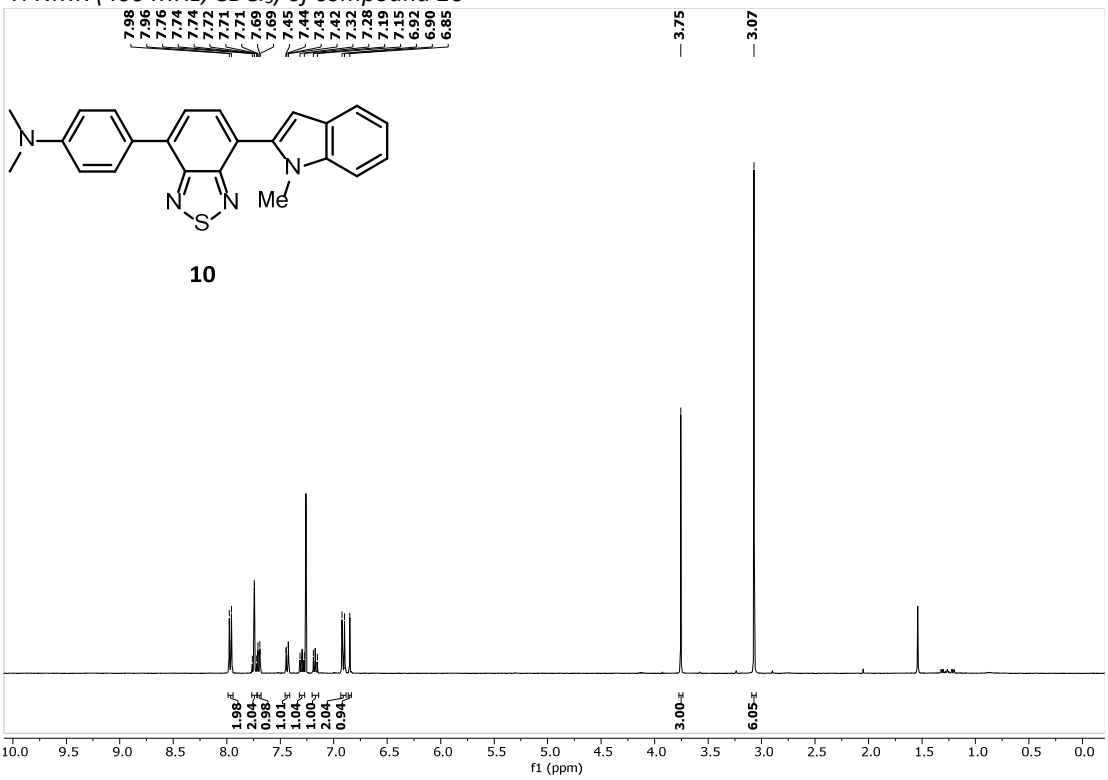

*^{13}C NMR (101 MHz, $CDCl_3$) of compound **10***

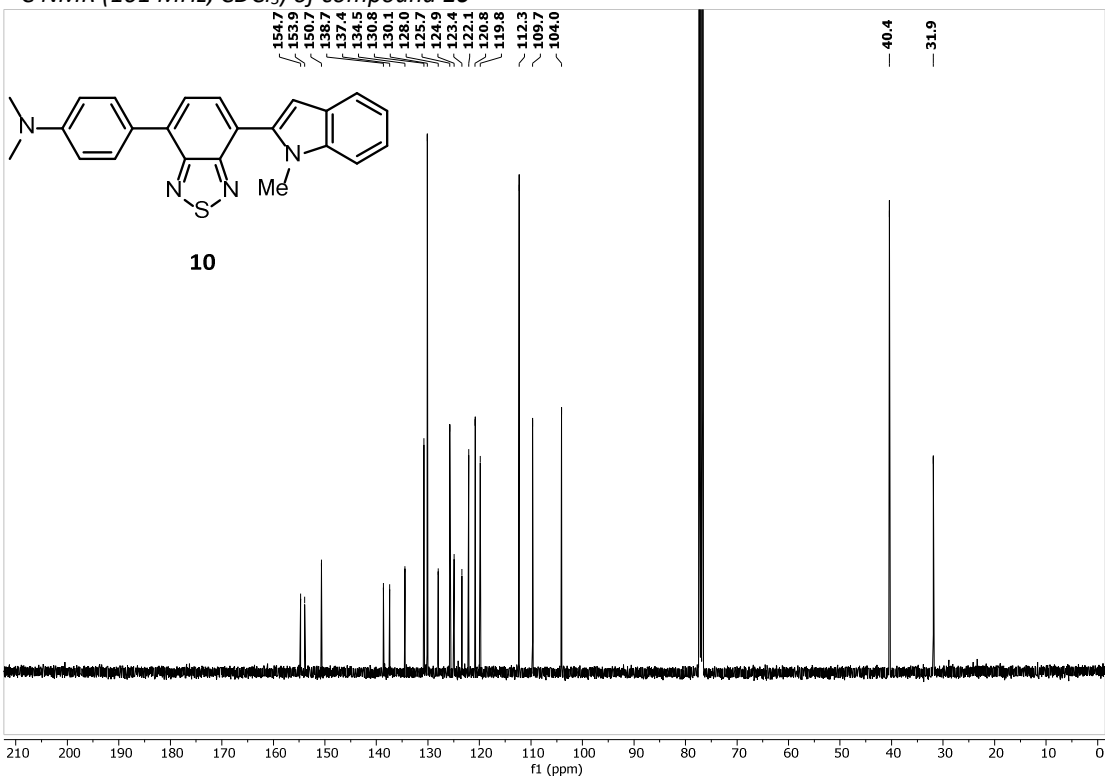

*^{1}H NMR (400 MHz, $CDCl_3$) of compound **11***

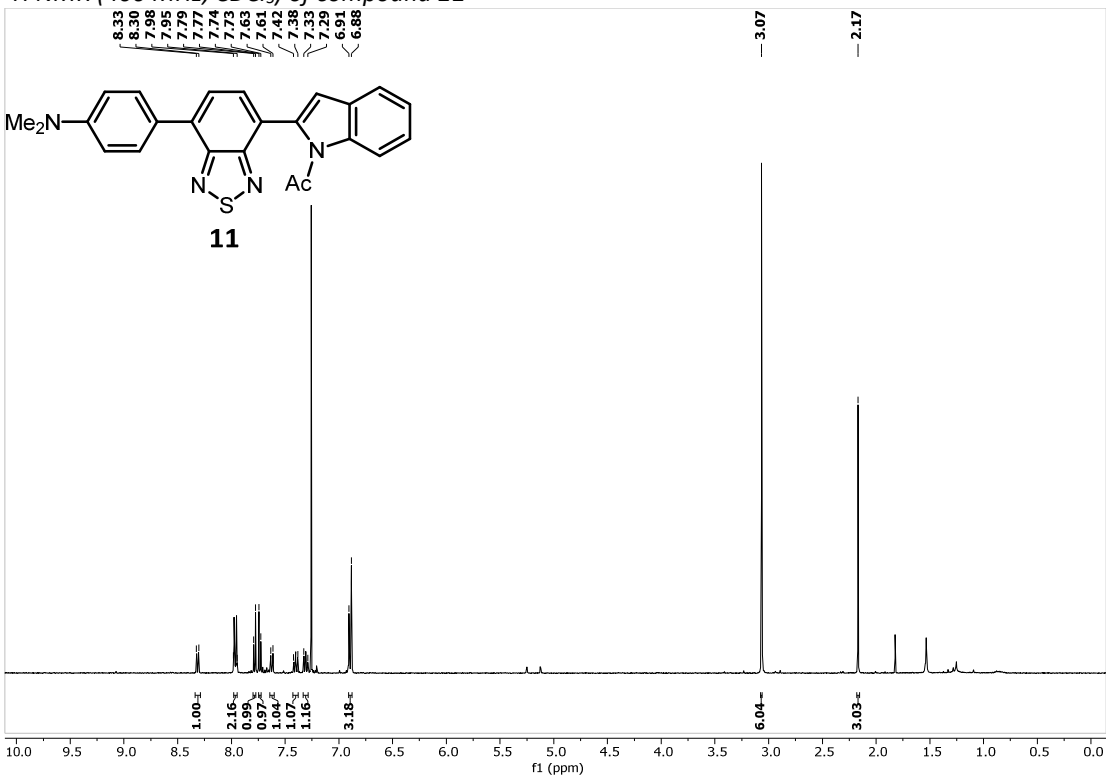

*^{13}C NMR (101 MHz, $CDCl_3$) of compound **11***

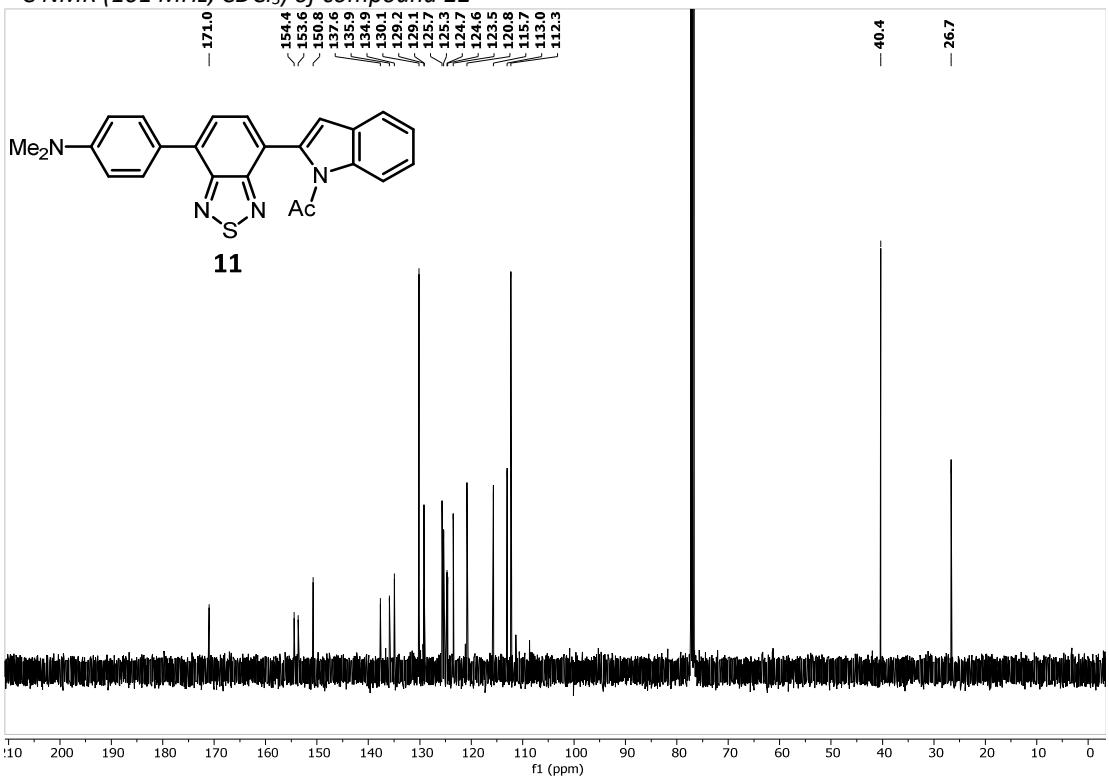

*^{1}H NMR (400 MHz, $CDCl_3$) of compound **12***

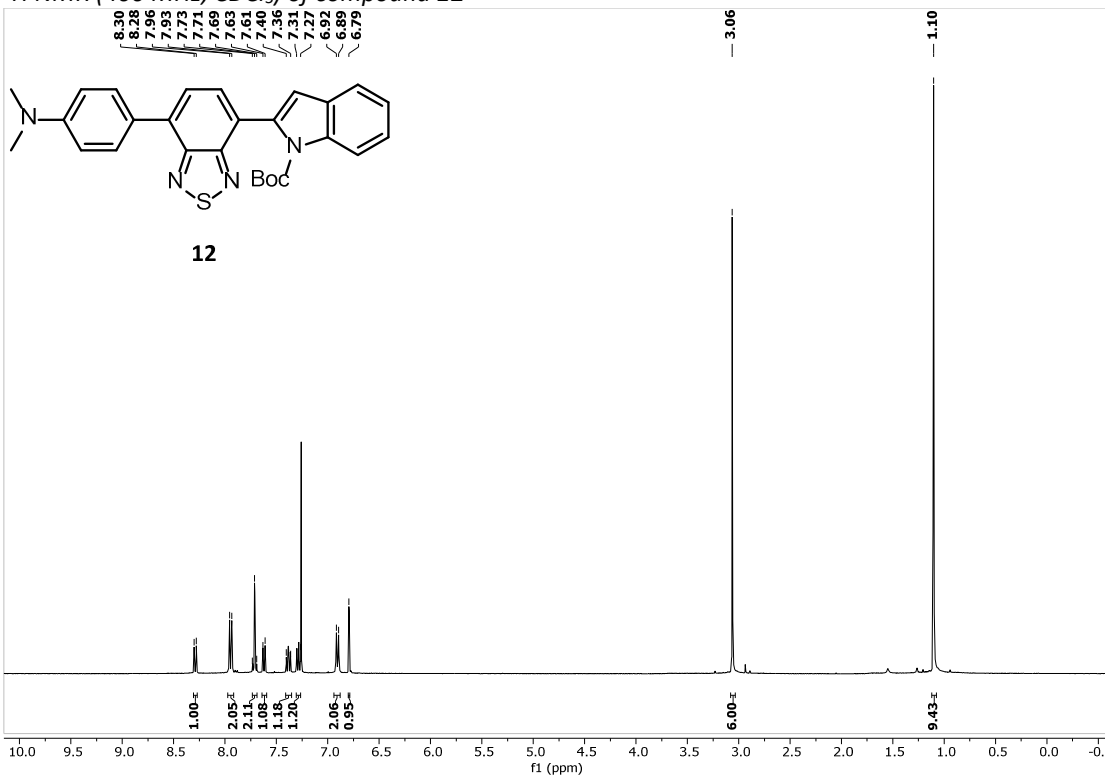

12

*^{13}C NMR (101 MHz, $CDCl_3$) of compound **12***

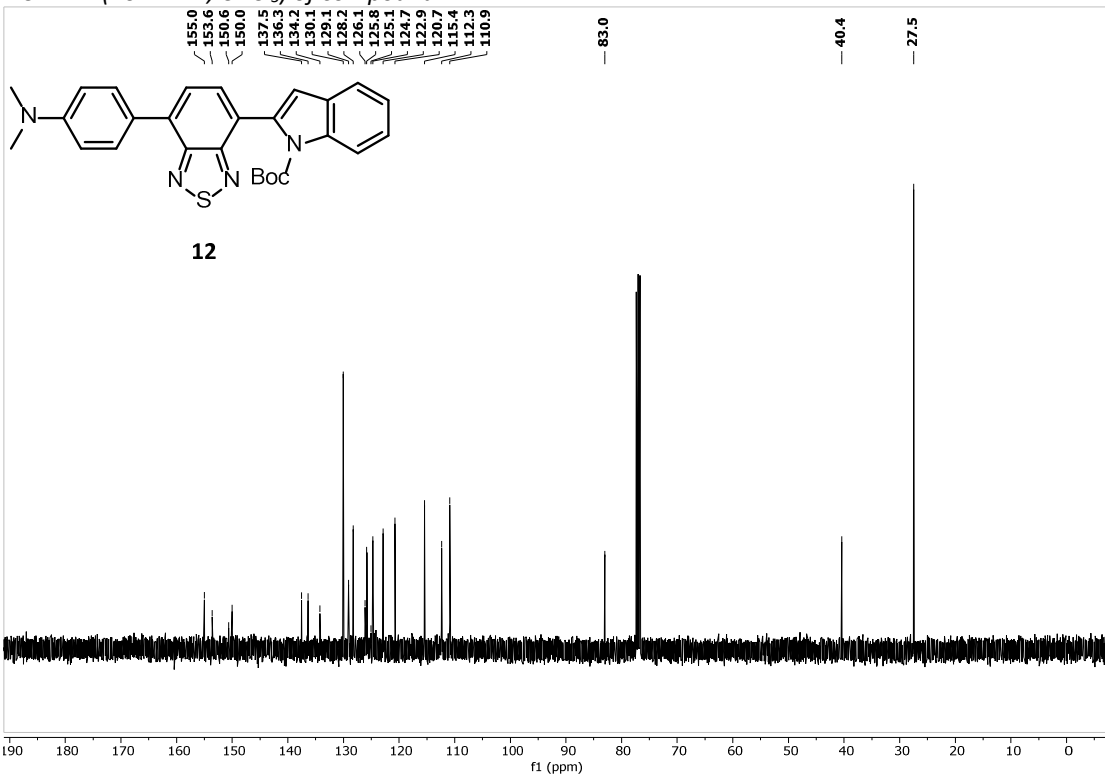

12